Crystal structures of boron-rich rare-earth borides

Takaho Tanaka

Scientific Information Office, National Institute for Materials Science

E-mail: tanaka.takaho@nims.go.jp

Abstract. Scandium, yttrium and heavy rare-earth elements (Gd-Lu) can form a variety of rare-earth boron compounds. When rich in boron, they often have complex crystal structures where boron icosahedra (B_{12}) are interconnected in various three-dimensional boron frameworks which accommodate metal atoms in their voids. Such structures are reviewed in this article.

1. Introduction

In metal-boron compounds, bonding of boron varies depending on the composition ratio [B]/[Me]. Diborides have ratio [B]/[Me] = 2, as in the well-known superconductor MgB_2; they crystallize in a hexagonal AlB_2-type layered structure. Hexaborides, i.e., [B]/[Me] = 6, form a three-dimensional boron framework whose structural unit is a boron octahedron. Tetraborides, i.e., [B]/[Me] = 4, are mixtures of diboride- and hexaboride structures. Dodecaborides, i.e., [B]/[Me] = 12, have a cubic lattice whose structure unit is a cubo-octahedron. When the composition ratio exceeds 12, boron forms B_{12} icosahedra which are linked into a three-dimensional boron framework, and the metal atoms reside in voids of this framework. Atomic structure of such B_{12} icosahedra-based borides will be the subject of this article. Figures 1a, b and c show the B_6 octahedron, B_{12} cubo-octahedron and B_{12} icosahedron, respectively.

This complicated bonding behavior originates from the fact that boron has only three valence electrons; this hinders tetrahedral bonding as in diamond or hexagonal bonding as in graphite. Instead, boron atoms form polyhedra. For example, three boron atoms form triangle, sharing two electrons to complete the so-called three-center bonding. Boron polyhedra, such as B_6 octahedron, B_{12} cubo-octahedron and B_{12} icosahedron, lack two valence electrons per polyhedron to complete the polyhedron-based framework structure. Metal atoms need to donate two electrons per boron polyhedron to form boron-rich metal borides. Thus, boron compounds are often regarded as electron deficient solids.

Initially, 8 crystal structure types of the icosahedral B_{12} compounds have been known:

(1) α-rhombohedral boron ($B_{13}C_2$)

(2) β-rhombohedral boron (MeB_x, $23 \leq x$)

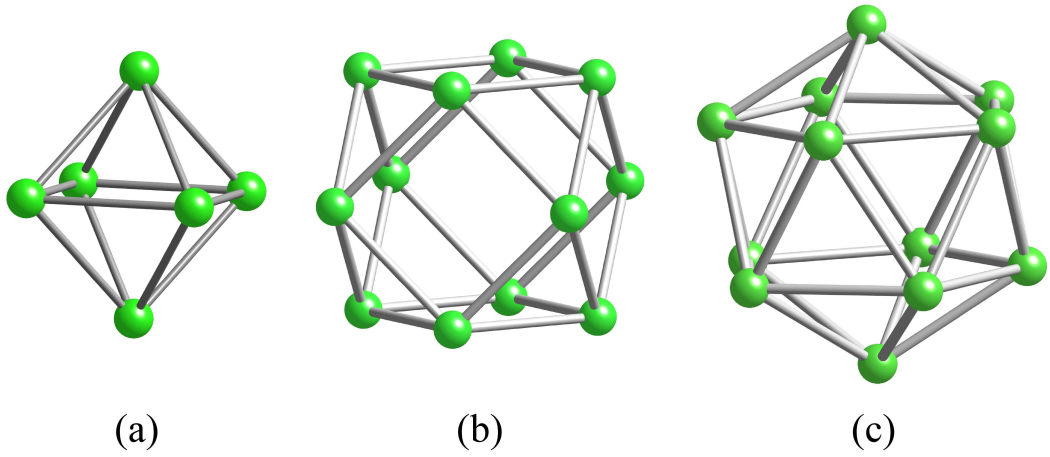

Figure 1. (a) B_6 octahedron, (b) B_{12} cubo-octahedron and (c) B_{12} icosahedron.

(3) α-tetragonal boron ($B_{48}B_2C_2$)
(4) β-tetragonal boron (β-AlB_{12})
(5) AlB_{10} or AlC_4B_{24}
(6) YB_{66}
(7) NaB_{15} or $MgAlB_{14}$
(8) γ-AlB_{12}.

Other structure types, BeB_3 [1] and SiB_6 [35], were characterized later. Thus only two kinds of boron-rich rare-earth borides have been known, namely $REAlB_{14}$ ($MgAlB_{14}$ structure type) and REB_{66} (YB_{66} structure type). We have grown single crystals of YB_{66} using floating zone technique aiming to develop a soft X-ray monochromator for dispersing synchrotron radiation in the energy range 1-2 keV. During the course of that work, two new binary compounds, YB_{25} and YB_{50}, have been discovered. Both compounds decompose at high temperatures without melting that hinders their growth as single crystals by floating zone method. However, we found that addition of a small amount of Si solves this problem and results in single crystals [3] with the stoichiometry of $YB_{41}Si_{1.2}$ [4]. This success opened a route to synthesize many new boron-rich rare-earth borides.

Albert and Hillebrecht comprehensively reviewed binary and selected ternary boron compounds containing main-group elements, namely, borides of the alkali and alkaline-earth metals, aluminum borides and compounds of boron and the nonmetals C, Si, Ge, N, P, As, O, S and Se [5]. They, however, excluded icosahedron-based rare-earth borides. Rare-earth elements have *d*- and *f*-electrons that complicated chemical and physical properties of rare-earth borides as compared to borides of main-group elements. Werheit *et al.* reviewed Raman spectra of numerous icosahedron-based boron compounds, which helps understanding the dynamic character of icosahedron-based frameworks [6].

This paper reviews crystal structures of newly found icosahedron-based rare-earth

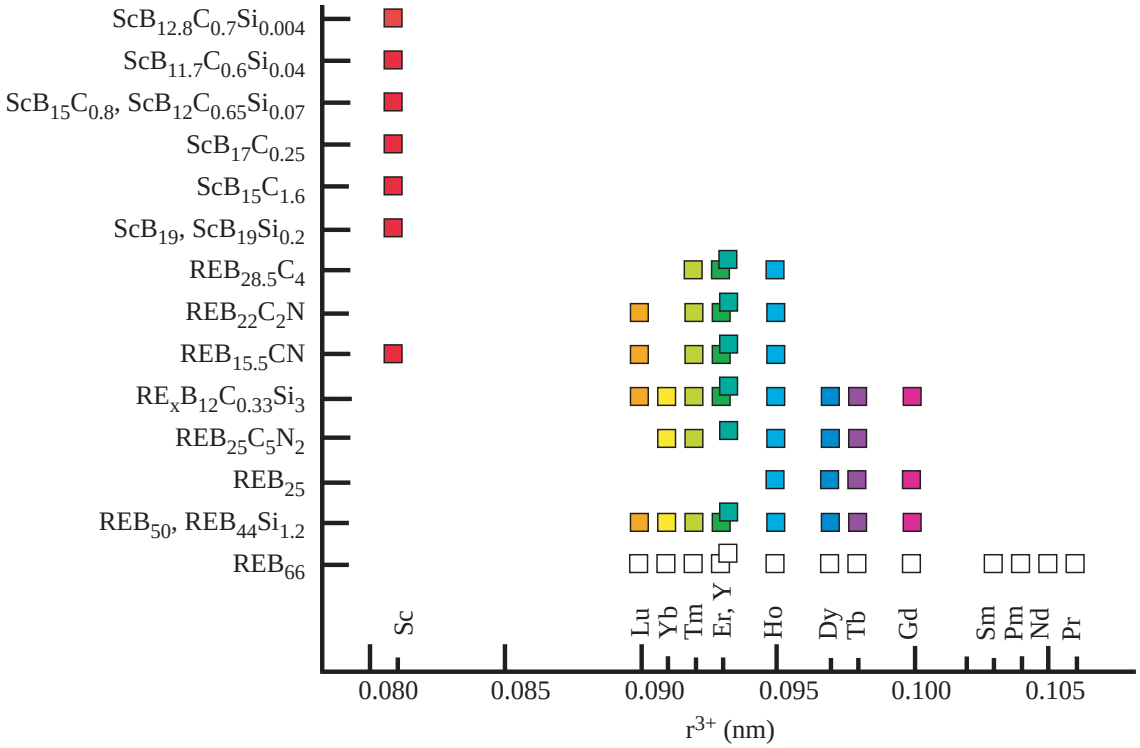

Figure 2. Relationship between the ionic radius of trivalent rare-earth ion and chemical composition of icosahedron-based rare-earth borides.

borides in addition to the previously known structure types of $REAlB_{14}$ and REB_{66}. Figure 2 shows a relationship between the ionic radius of trivalent rare-earth ions and the composition of some rare-earth borides. First, crystal structures of borides of yttrium and heavy rare-earth metals will be introduced. Scandium has many unique boron compounds, as shown in figure 2, because of the much smaller ionic radius compared with other rare-earth elements. The crystal structures of Sc compounds will be described second.

In understanding the crystal structures described in this article, it is important to keep in mind the concept of partial site occupancy, that is, some atoms in the described below unit cells can take several possible positions with a given statistical probability. Thus, on the basis of the given statistical probability, some of the partial-occupancy cites in such a unit cell are empty, and the remained cites are occupied.

2. $REAlB_{14}$ and REB_{25}

$REAlB_{14}$ and REB_{25} compounds have the $MgAlB_{14}$ structure which has orthorhombic symmetry and space group *Imma* (No. 74). In this structure, rare-earth atoms enter the Mg site. Aluminium sites are empty for REB_{25}, which can also be described as $RE\sqcup B_{14}$. Both metal sites of $REAlB_{14}$ structure have partial occupancies around 60∼70% and the REB_{25} formula merely reflects the average atomic ratio [B]/[RE] = 25.

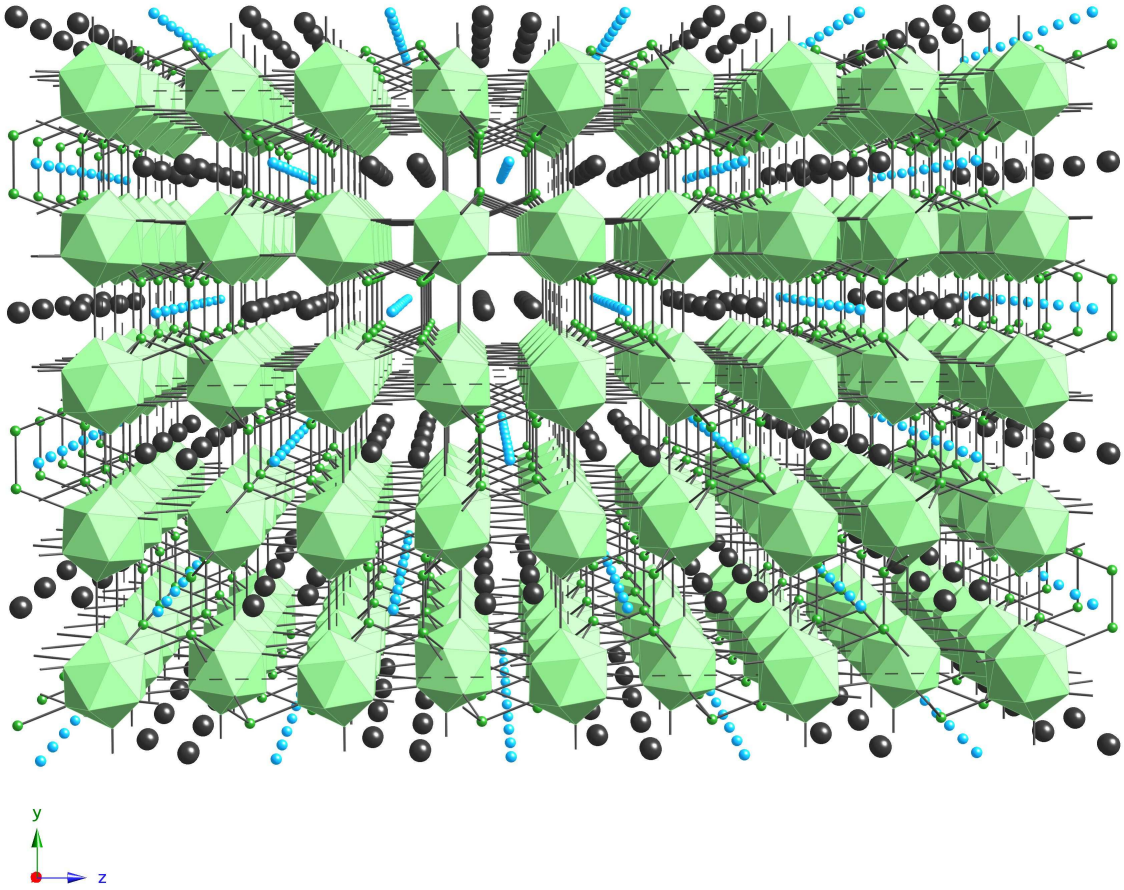

Figure 3. Crystal structure of $YAlB_{14}$. Black and blue spheres indicate Y and Al atoms, respectively. Vacancies at the Y and Al sites are ignored.

Yttrium borides form both $YAlB_{14}$ and YB_{25} structures. Experiments have confirmed that the borides based on rare-earth elements from Tb to Lu can have the $REAlB_{14}$ structure [7, 8, 9, 10]. A subset of these borides containing rare-earth elements from Gd to Er can also crystallize in the REB_{25} structure [11].

Korsukova *et al* [9] analyzed the $YAlB_{14}$ crystal structure using a single crystal grown by the high-temperature solution-growth method. The lattice constants were deduced as $a = 0.58212(3)$, $b = 1.04130(8)$ and $c = 0.81947(6)$ nm, and the atomic coordinates and site occupancies are summarized in Appendix I.

Figure 3 shows crystal structure of $YAlB_{14}$ viewed along the x-axis. The large black spheres are Y atoms, the small blue spheres are Al atoms and the small green spheres are the bridging boron sites. B_{12} clusters are depicted as the green icosahedra. Boron framework of $YAlB_{14}$ is one of the simplest among icosahedra-based borides - it consists of only one kind of icosahedra and one bridging boron site. The bridging boron site is tetrahedrally coordinated by four boron atoms, i.e., by another boron atom in the counter bridge site, and three boron atoms, each of which is an equatorial atom of one of three B_{12} icosahedra. Aluminium atoms are separated by 0.2911 nm

and are arranged in lines parallel to the x-axis, whereas yttrium atoms are separated by 0.3405 nm. Both the Y atoms and B_{12} icosahedra form zigzags along the x-axis. As described above, the bridging boron atoms connect three equatorial boron atoms of three icosahedra and those icosahedra form a network parallel to the (101) crystal plane (x-z plane in the figure). The bonding distance between the bridging boron and the equatorial boron atoms is 0.1755 nm, which is typical for the strong covalent B-B bond (bond length 0.17-0.18 nm); thus, the bridging boron atoms contribute to strengthening the individual network planes. On the other hand, the large distance between the boron atoms within the bridge (0.2041 nm) suggests weaker interaction, and thus the bridging sites contribute little to the bonding between the network planes.

The boron framework of $YAlB_{14}$ needs donation of four electrons from metal elements: two electrons for a B_{12} icosahedron and one electron for each of the two bridging boron atoms, to support their tetrahedral coordination. The real chemical composition of $YAlB_{14}$, determined by the structure analysis, is $Y_{0.62}Al_{0.71}B_{14}$ as described in the Appendix I. If both metal elements are trivalent ions then 3.99 electrons can be transferred to the boron framework, which is very close to the required value of 4. However, because the bonding between the bridging boron atoms is weaker than in a typical B-B covalent bond, less than 2 electrons are donated to this bond, and metal atoms need not be trivalent. On the other hand, the electron transfer from metal atoms to the boron framework implies that not only strong covalent B-B bonding within the framework but also ionic interaction between metal atoms and the framework contribute to the $YAlB_{14}$ phase stabilization.

3. REB_{66}-type borides

In addition to yttrium, a wide range of rare-earth elements from Nd to Lu, except for Eu, can form REB_{66} compounds [12]. Seybolt discovered the compound YB_{66} in 1960 [13] and its structure was solved by Richards and Kasper in 1969 [14]. They reported that YB_{66} has a face-centered cubic structure with space group $Fm\overline{3}c$ (No. 226) and lattice constant $a = 2.3440(6)$ nm. There are 13 boron sites B1-B13 and one yttrium site. The B1 sites form one icosahedron and the B2 to B9 sites form another icosahedron. These icosahedra arrange in a thirteen-icosahedron unit $(B_{12})_{12}B_{12}$ which is shown in figure 4(a) and is called supericosahedron. The icosahedron formed by the B1 site atoms is located at the center of the supericosahedron. The supericosahedron is one of the basic units of the boron framework of YB_{66}. There are two types of supericosahedra: one occupies the cubic face centers and another, which is rotated by 90°, is located at the center of the cell and at the cell edges. Thus, there are eight supericosahedra (1248 boron atoms) in the unit cell.

Another structure unit of YB_{66}, shown in figure 4(b), is B_{80} cluster of 80 boron sites formed by B10 to B13 [15]. All those cites are partially occupied and in total contain only about 42 boron atoms. The B_{80} cluster is located at the body center of the octant of the unit cell, i.e., at the 8a position (1/4, 1/4, 1/4); thus, there are eight such clusters

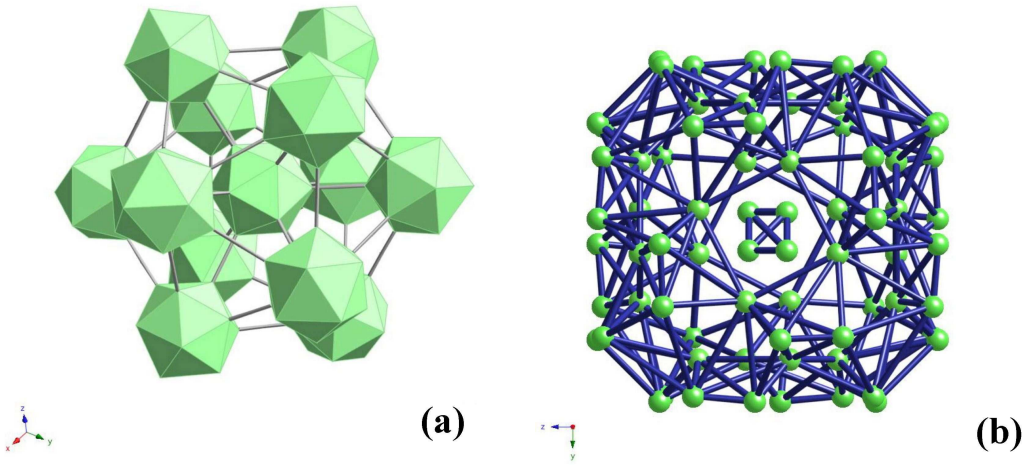

Figure 4. (a) Thirteen-icosahedron unit $(B_{12})_{13}B_{12}$ (supericosahedron), and (b) B_{80} cluster unit. The excessive bonding in panel (b) is because it assumes that all sites are occupied, whereas the total number of boron atoms is only 42.

(336 boron atoms) per unit cell. Two independent structure analyses [14, 15] came to the same conclusion that the total number of boron atoms in the unit cell is 1584. The boron framework structure of YB_{66} is shown in figure 5(a). To indicate relative orientations of the supericosahedra, a schematic drawing is shown in figure 5(b), where the supericosahedra and the B_{80} clusters are depicted by light green and dark green spheres, respectively; at the top surface of the unit cell, the relative orientations of the supericosahedra are shown by arrows.

There are 48 yttrium sites ((0.0563, 1/4, 1/4) for YB_{62} [15]) in the unit cell. Richards and Kasper fixed the Y site occupancy to 0.5 that resulted in 24 Y atoms in the unit cell and the chemical composition of YB_{66} [14]. As shown in figure 6, Y sites form a pair separated by only 0.264 nm in YB_{62}. This pair is aligned normal to the plane formed by four supericosahedra. The Y site occupancy 0.5 implies that the pair has always one Y atom with one empty site.

Slack *et al* have reported an interesting fact that the total number of boron atoms in the unit cell, calculated from the measured values of density, chemical composition and lattice constant, is approximately 1628 ± 4 [16], which is about 3% larger than the value 1584 obtained from the structure analyses [14, 15]. I confirmed the fact and found that the number of B atoms in the unit cell remains nearly constant when the chemical composition changes from YB_{56} to YB_{66}. On the other hand, the total number of yttrium atoms per unit cell varies, and it is, for example, $\sim$26.3 for YB_{62} (see table 1). This discrepancy between the structure and density analyses on Y and B atom numbers in the unit cell motivated us to reinvestigate the YB_{66} crystal structure. We have successfully reproduced chemical composition of YB_{56} and YB_{62} by introducing a trivalent Y ion instead of neutral Y atom into the structure analysis [15]. However,

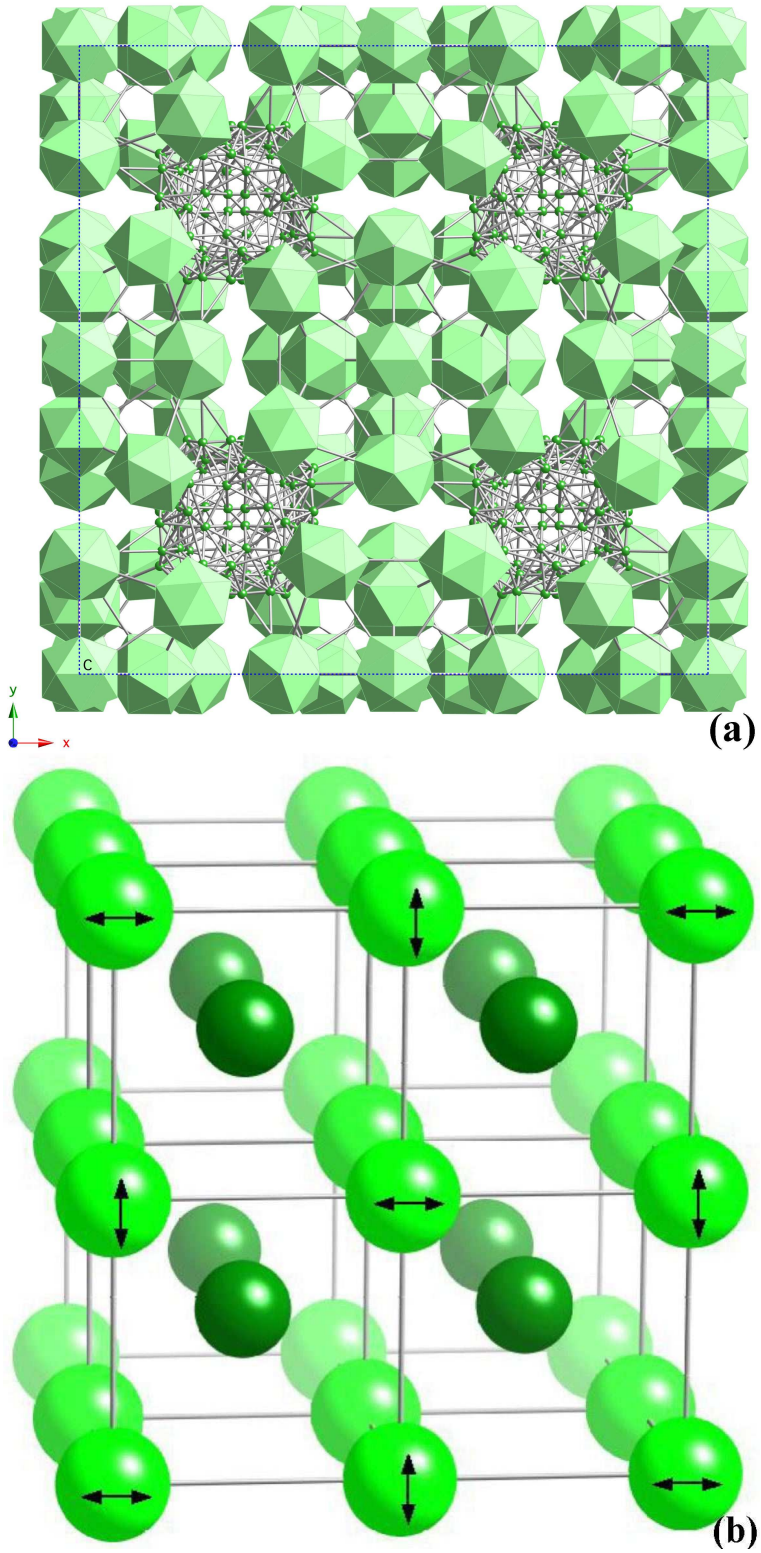

Figure 5. (a) The boron framework of YB_{66} viewed along the z-axis. (b) Schematically drawn boron framework of YB_{66}. Light green spheres show the boron supericosahedra and their relative orientations are indicated by arrows. Dark green spheres correspond to the B_{80} clusters.

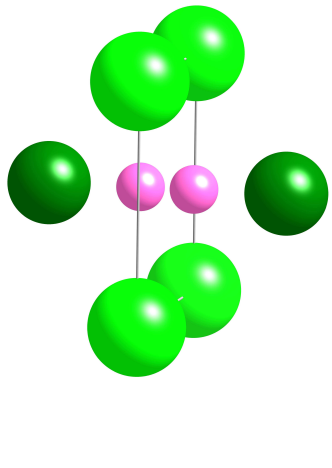

Figure 6. Pair of Y sites (pink spheres) in YB_{66}. Light green spheres show the boron supericosahedron and dark green spheres correspond to the B_{80} clusters.

the total number of B atoms in the unit cell remained the same as that obtained by Richards and Kasper and the total number of Y atoms was no more than 25.3 for YB_{62}, which could not reproduce the experimental values shown in table 1.

Table 1. Number of B, Y and Mo or Pt atoms in the unit cell obtained from experimental data on chemical composition, lattice constant and density [17].

Composition	a(nm)	ρ(g/cm^3)	N_B	N_Y	$N_{Mo/Pt}$
YB_{66} [14]	2.3440	2.52	1610	24.4	-
$YB_{61.754}$ [16]	2.3445	2.5687	1628	26.4	-
YB_{62}	2.34364	2.5662	1624	26.2	-
YB_{56}	2.34600	2.5927	1626	29.0	-
$YMo_{0.20}B_{62.4}$	2.34258	2.64	1628	26.1	5.3
$YPt_{0.091}B_{63.5}$	2.34300	2.6344	1634	25.7	2.4
$YPt_{0.096}B_{63.3}$	2.34223	2.6355	1630	25.7	2.5
$YPt_{0.14}B_{62.0}$	2.34055	2.6762	1629	26.3	3.7

If the total number of Y atoms stays bellow or equal to 24 then it is possible that one Y atom accommodates in each Y pair. However, the experimental value of 26.3 significantly exceeds 24, and thus both pair sites might be occupied. In this case, because of the small separation between the two Y atoms, they must be repelled by Coulomb force. To clarify this point, we repeated the structure analysis introducing split Y sites and found better agreement with the experiment [18]. The Y site distances

and occupancies are presented in table 2.

Table 2. x-coordinates and occupancies of Y1 and Y2 sites.

Atom	x	Occupancy
Y1	0.0542(3)	0.437(9)
Y2	0.0725(11)	0.110(12)

There are twenty Y pair sites with one Y atom and three pairs with two Y atoms. Interestingly, there is also one empty Y pair. The separation 0.340 nm for the Y2 pair site (two Y atoms in the pair site) is much larger than the separation 0.254 nm for the Y1 pair site (one Y atom in the pair site), as expected. The total number of Y atoms in the unit cell is 26.3, exactly as measured. Both cases are compared in figure 7. The larger separation for the Y2 pair site is clear as compared with that for the Y1 pair site. In case of the Y2 pair, some neighboring boron sites that belong to the B_{80} cluster must be unoccupied because they are too close to the Y2 site.

Splitting the Y site yielded right number of Y atoms, but not B atoms in the unit cell. Not only the occupation of the B sites in the B_{80} cluster must be strongly dependent on whether or not the Y site is the Y1 state or the Y2 state, but also the position of the occupied B sites must be affected by the state of the Y site. However, it was difficult to introduce split positions to individual B sites because the existence of the residual electron density was not so clear. Introduction of the split Y sites has improved the *R1* value of the structure analysis from about 6 to 5%. The 5% value is still not satisfactory, and this is probably due to the difficulty of counting correct B occupation at each site. In most other structure analyses of the icosahedron-based rare-earth borides we could reduce the *R1* value to less than 4% without a need to introduce the split metal site.

Atomic coordinates and site occupancies are summarized in Appendix II.

4. $REB_{41}Si_{1.2}$

Similar to yttrium, rare-earth metals from Gd to Lu can form $REB_{41}Si_{1.2}$-type boride. At first, this compound was found as YB_{50} that was synthesized by solid-state reaction [19]. X-ray powder diffraction (XRD) and electron diffraction indicated that YB_{50} has an orthorhombic structure with lattice constants a = 1.66251(9), b = 1.76198 and c = 0.94797(3) nm. The space group was assigned as $P2_12_12$ [19]. Because of the close similarity in lattice constants and space group, we have expected that YB_{50} has the γ-AlB_{12}-type orthorhombic structure whose lattice constants and space group are a = 1.6573(4), b = 1.7510(3) and c = 1.0144(1) nm and $P2_12_12$ [20]. YB_{50} decomposes at ∼1750 °C without melting that hinders growth of single crystals from the melt. Small amounts of Si addition made YB_{50} to melt without decomposition, which enabled single-crystal growth from the melt [3] and single-crystal structure analysis as well [4].

Structure analysis indicated that $YB_{41}Si_{1.2}$ has not the γ-AlB_{12}-type lattice but a new orthorhombic crystal structure (space group: *Pbam*, No. 55) with lattice constants

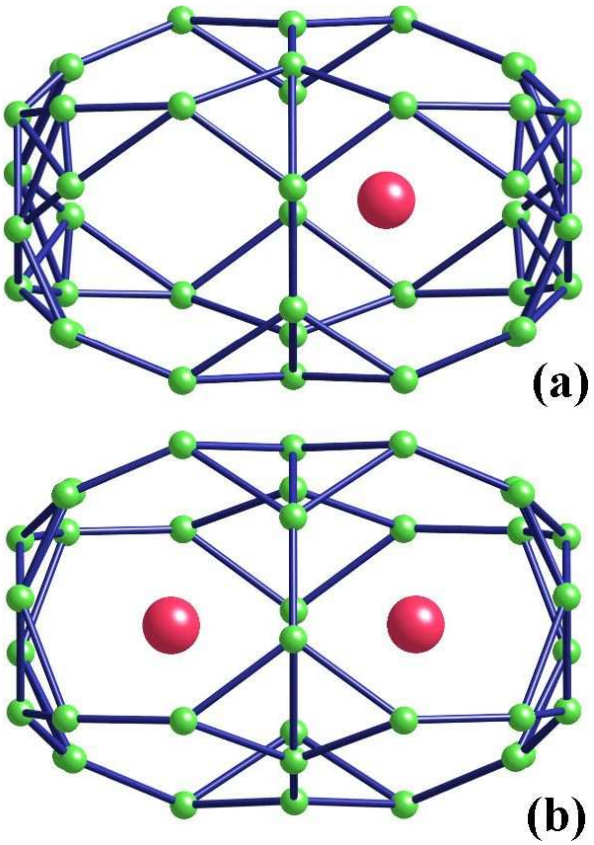

Figure 7. Two cases of the Y pair sites: with one Y atom (top) and two Y atoms (bottom). In the latter case, some neighboring boron sites are eliminated because they are too close to the Y site.

of $a = 1.674(1)$ nm, $b = 1.7667(1)$ nm and $c = 0.9511(7)$ nm [4]. There are 58 independent atomic sites in the unit cell. Three of them are occupied by either B or Si atoms (mixed-occupancy sites), one is a Si bridge site and one is Y site. From the remaining 53 boron sites, 48 form icosahedra and 5 are bridging sites. Atomic coordinates and site occupancies are summarized in Appendix III.

The boron framework of $YB_{41}Si_{1.2}$ consists of five B_{12} icosahedra (I1-I5) and a $B_{12}Si_3$ polyhedron shown in figure 8(a). An unusual linkage between two icosahedra is depicted in figure 8(b), where two B_{12}-I5 icosahedra connect via two B atoms of each icosahedron forming an imperfect square. The boron framework of $YB_{41}Si_{1.2}$ can be described as a layered structure where two boron networks stack along the z-axis. One boron network consists of 3 icosahedra I1, I2 and I3 and is located in $z = 0$ plane; another network consists of the icosahedron I5 and the $B_{12}Si_3$ polyhedron and lies at $z = 0.5$. The icosahedron I4 bridges these networks, and thus its height along the z-axis is 0.25. Both these networks are shown in figures 9(a) and (b).

The I4 icosahedra link two networks along the c-axis and therefore form an infinite chain of icosahedra along this axis as shown in figure 10. The unusually short distances (0.4733 and 0.4788 nm) between the neighboring icosahedra in this direction result in

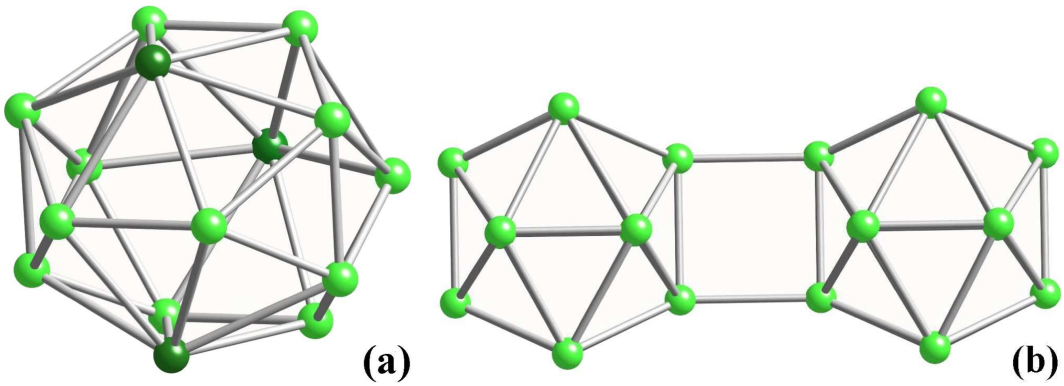

Figure 8. (a) $B_{12}Si_3$ polyhedron unit. Darker green spheres represent the sites which are occupied either by Si or B atoms. (b) Unusual linkage between the B_{12}-I5 icosahedra connected via two apex atoms of each icosahedron.

the relatively small c-axis lattice constant of 0.95110(7) nm in this compound - other borides with a similar icosahedral chain have this value larger than 1.0 nm. However, the bonding distances between the apex B atoms (0.1619 and 0.1674 nm) of neighboring I4 icosahedra are usual.

Another interesting feature of $YB_{41}Si_{1.2}$ is the 100% site occupancy of the Y site. In most icosahedron-based metal borides, metal sites have rather low site occupancy, for example, about 50% for YB_{66} and 60-70% for $REAlB_{14}$. When the Y site is replaced by rare-earth elements, $REB_{41}Si_{1.2}$ can have an antiferromagnetic-like ordering because of this high site occupancy [21, 22, 23].

5. Homologous icosahedron-based rare-earth borides

Rare-earth borides $REB_{15.5}CN$, $REB_{22}C_2N$ and $REB_{28.5}C_4$ are homologous with B_4C. B_4C has a typical crystal structure of an icosahedron-based compounds as shown in figure 11(a). There B_{12} icosahedra form a rhombohedral lattice unit (space group: $R\overline{3}m$ (No. 166), lattice constants: $a = 0.56$ nm and $c = 1.212$ nm) surrounding a C-B-C chain that resides at the center of the lattice unit, and both C atoms bridge the neighboring three icosahedra. This structure is layered: as shown in figure 11(b), B/12 icosahedra and bridging carbons form a network plane that spreads parallel to the c-plane and stacks along the c-axis.

These homologous compounds have two basic structure units - the B_{12} icosahedron and the B_6 octahedron. The network plane of B_4C structure can be periodically replaced by a B_6 octahedron layer so that replacement of every third, fourth and fifth layer would correspond to $REB_{15.5}CN$, $REB_{22}C_2N$ and $REB_{28.5}C_4$, respectively. B_6 octahedron is smaller than B_{12} icosahedron; therefore, rare-earth elements can reside in the space created by the replacement. The stacking sequences of B_4C, $REB_{15.5}CN$, $REB_{22}C_2N$ and $REB_{28.5}C_4$ are shown in figure 12(a), (b), (c) and (d), respectively. High-resolution transmission electron microscopy (HRTEM) lattice images of the latter three compounds

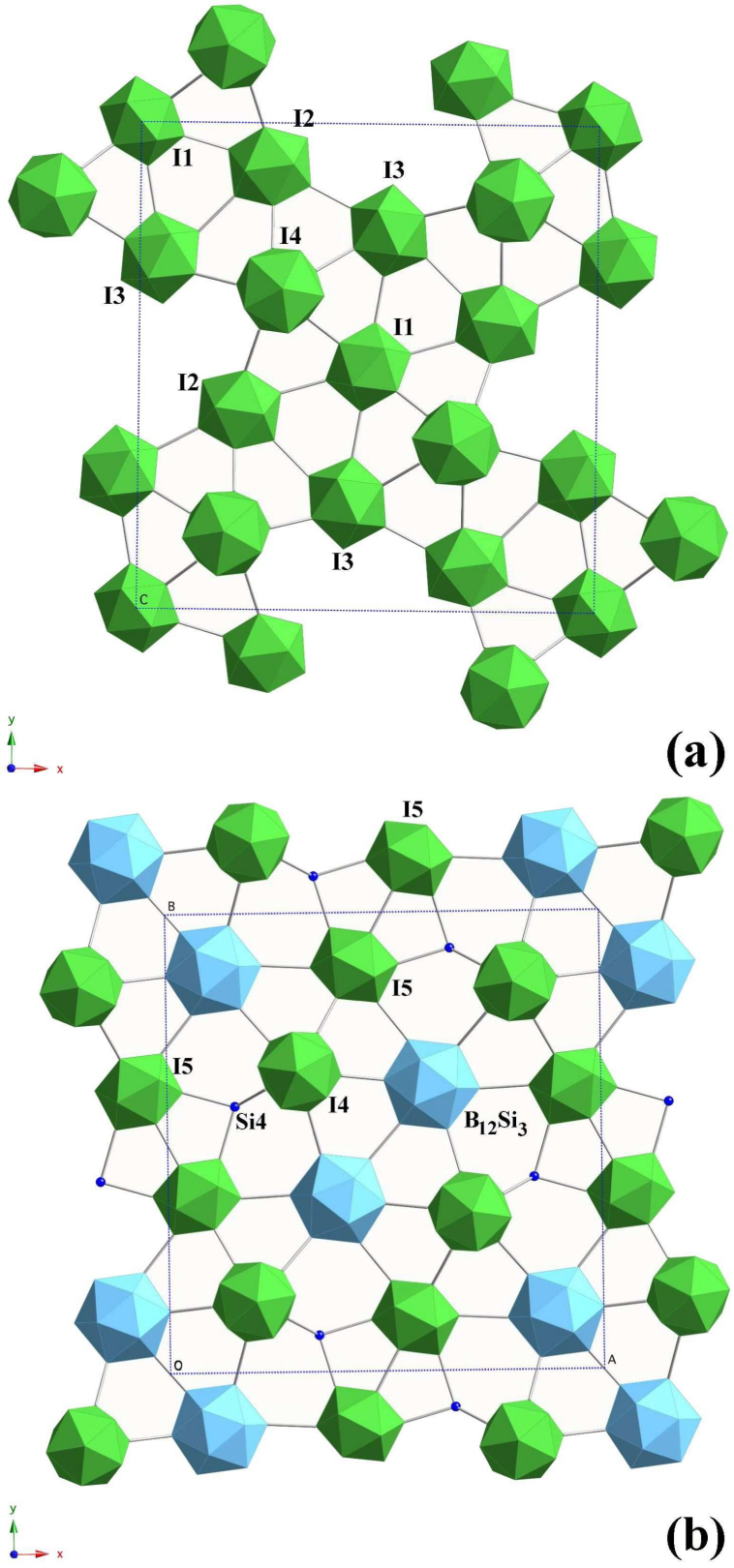

Figure 9. (a) The boron network that consists of the icosahedra I1, I2 and I3 and is located at $z = 0$ plane. The icosahedron I4 lies above and below of this network at $z = \pm 0.25$. (b) The boron network that consists of the I5 icosahedron and $B_{12}Si_3$ polyhedron (blue) and is located at $z = 0.5$ plane. The icosahedron I4 lies above and below this network at $z = 0.25$ and 0.75.

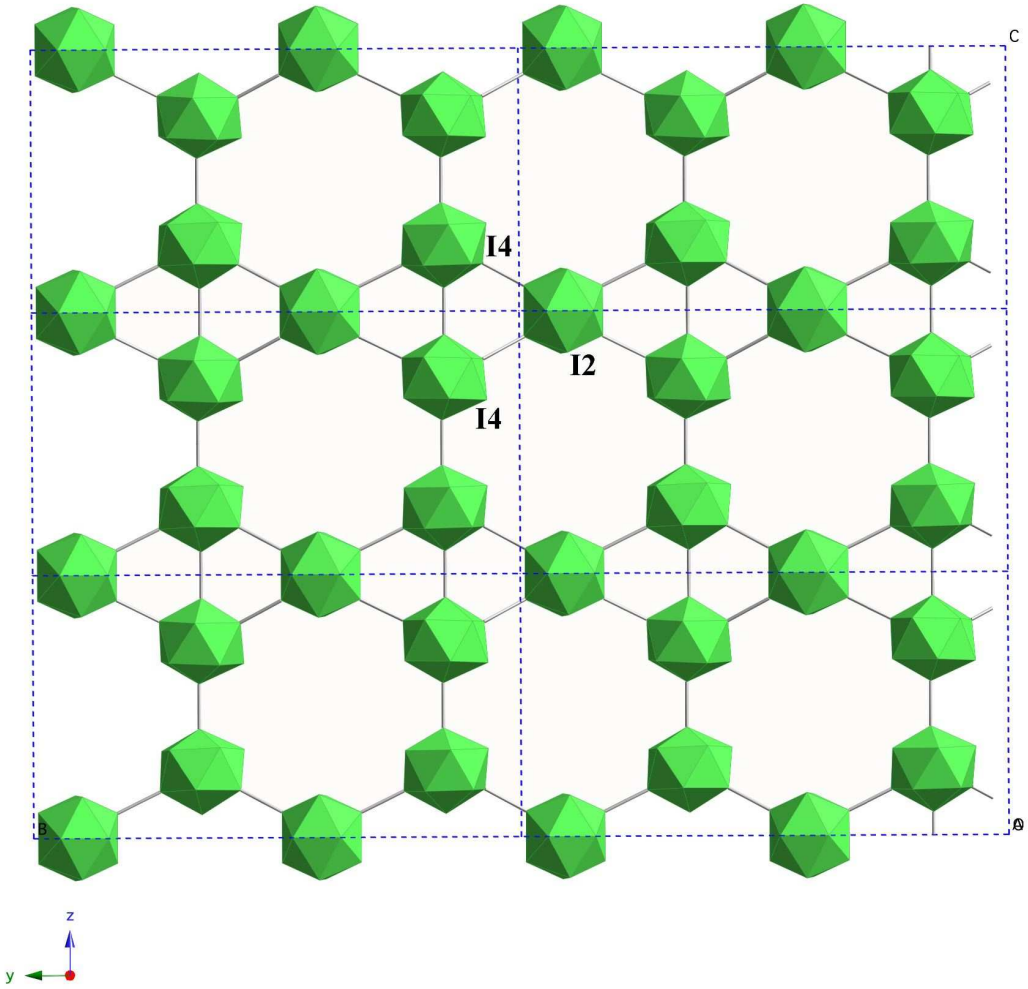

Figure 10. The *b*-*c* network formed by icosahedra I4 and I2 as seen along the *a*-axis. The network is drawn within the range $x = 0.09$-0.41.

are arranged by each side and do confirm the stacking sequence of each compound. The symbols 3T, 12R and 15R in brackets indicate the number of layers necessary to complete the stacking sequence, and T and R refer to trigonal and rhombohedral. Thus, $REB_{22}C_2N$ and $REB_{28.5}C_4$ have rather large *c*-lattice constants.

Because of the small size of the B_6 octahedra, they cannot interconnect. Instead, they bond to the B_{12} icosahedra in the neighboring layer, and this decreases bonding strength in the *c*-plane. Nitrogen atoms strengthen the bonding in the *c*-plane by bridging three icosahedra, like C atoms in the C-B-C chain. Figure 13 depicts the *c*-plane network revealing the alternate bridging of the boron icosahedra by N and C atoms. Decreasing the number of the B_6 octahedra diminishes the role of nitrogen

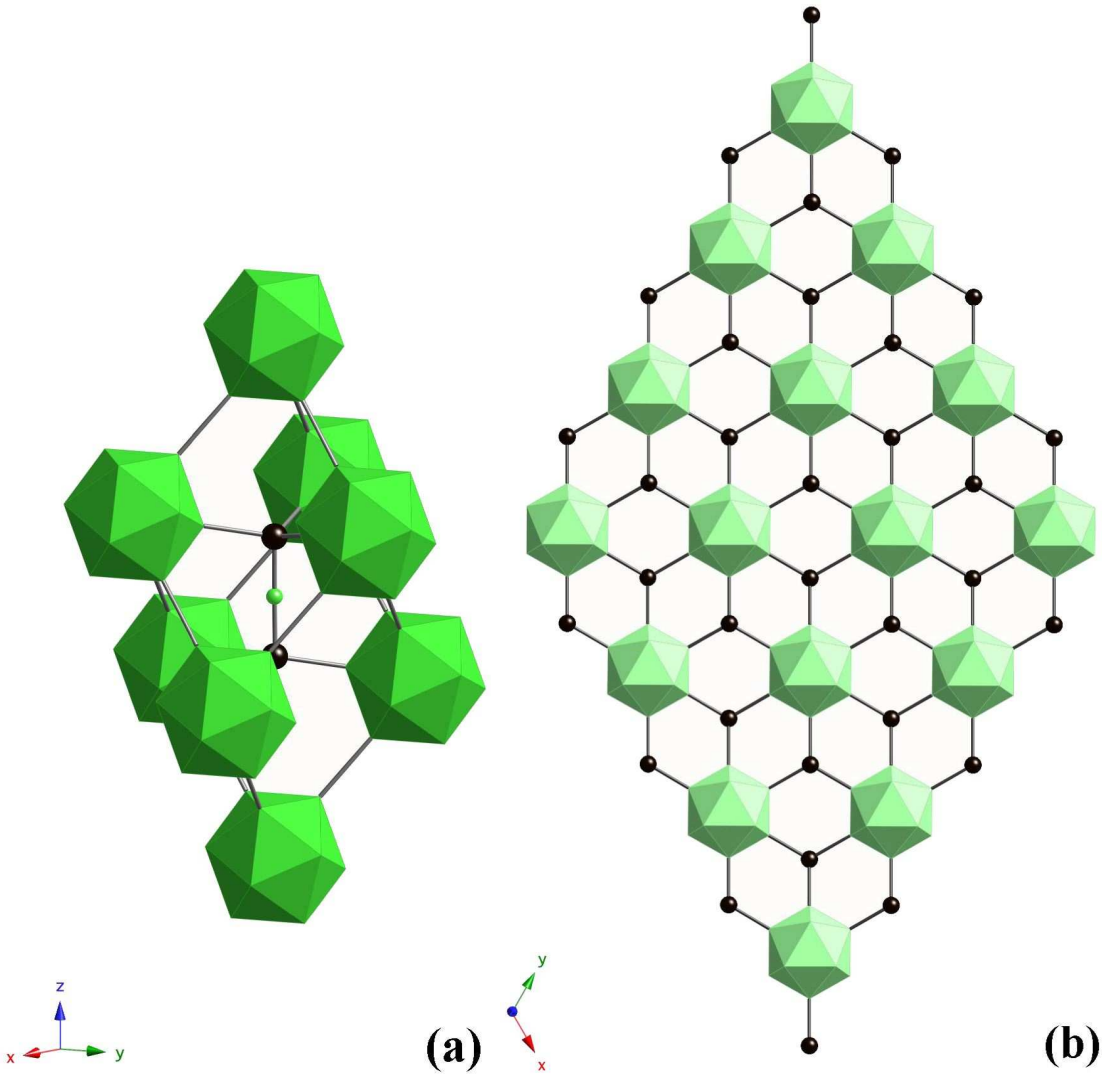

Figure 11. (a) Structure unit of B_4C and (b) *c*-plane network of B_{12} icosahedra in the B_4C structure.

because the C-B-C chains start bridging the icosahedra. On the other hand, in MgB_9N, in which the B_6 octahedron layer and the B_{12} icosahedron layer stack alternatively and there is no C-B-C chains [24], only N atoms bridge the B_{12} icosahedra. However, REB_9N compounds have not been identified yet.

Sc, Y, Ho, Er, Tm and Lu are confirmed to form $REB_{15.5}CN$-type compounds [25]. Single-crystal structure analysis has been carried out for $ScB_{15.5}CN$ and yielded trigonal symmetry (space group $P\overline{3}m1$ (No.164) with $a = 0.5568(2)$ and $c = 1.0756(2)$ nm). Atomic coordinates of $ScB_{15.5}CN$ are summarized in Appendix IVa.

$REB_{22}C_2N$ was synthesized for Y, Ho, Er, Tm and Lu [26]. The crystal structure, solved for the representative compound $YB_{22}C_2N$, belongs to the trigonal with space group $R\overline{3}m$ (No.166); it has six formula units in the unit cell and lattice constants $a = b = 0.5623(0)$ nm and $c = 4.4785(3)$ nm. Atomic coordinates of $YB_{22}C_2N$ are summarized

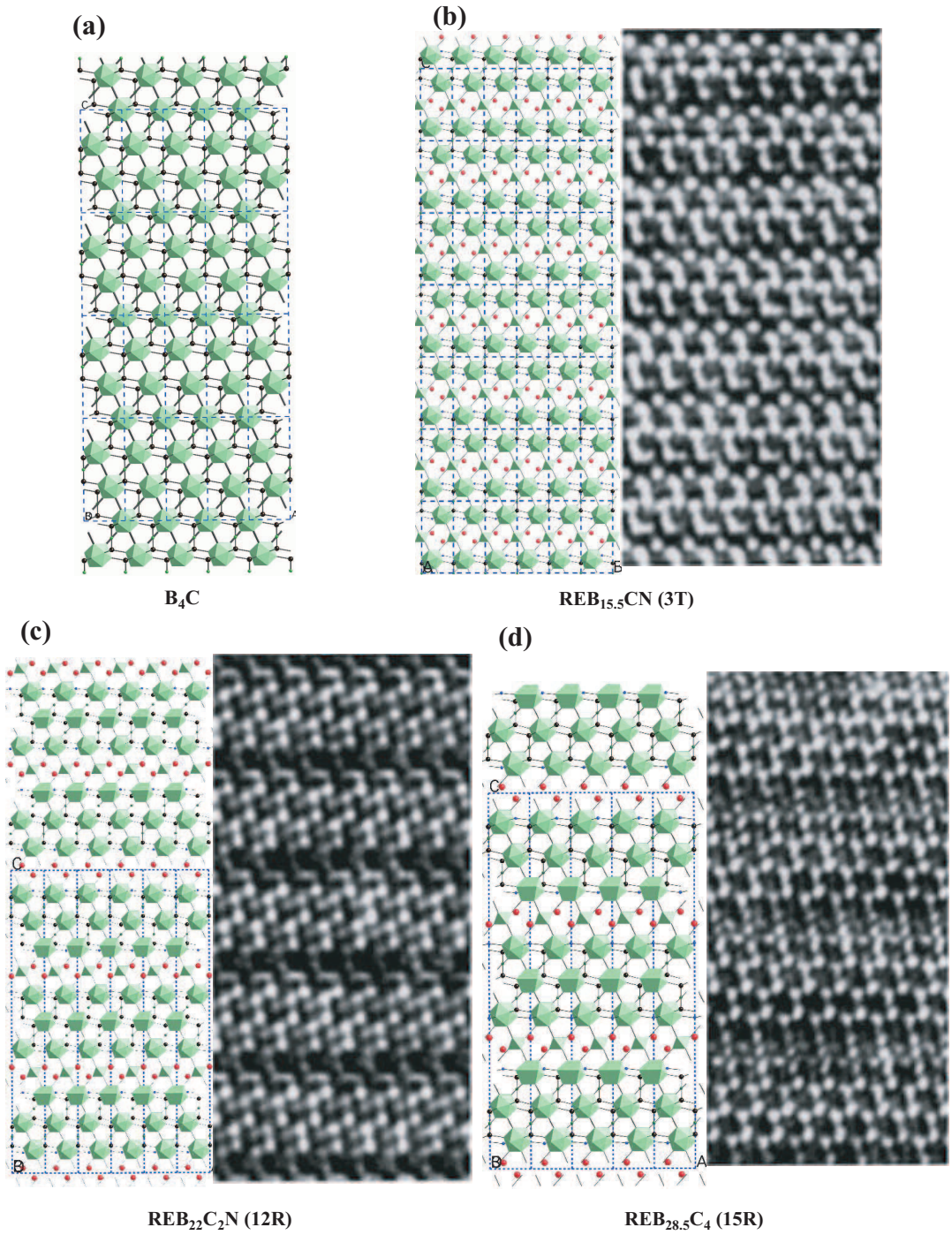

Figure 12. (a) Stacking sequences of homologous icosahedron-based rare-earth borides and their HRTEM lattice images; (a) B_4C, (b) $REB_{15.5}CN$ (3T), (c) $REB_{22}C_2N$ (12R) and (d) $REB_{28.5}C_4$ (15R). Red circles are rare-earth atoms. HRTEM lattice images were obtained for $YB_{15.5}CN$, $YB_{22}C_2N$ and $YB_{28.5}C_4$ compounds [28].

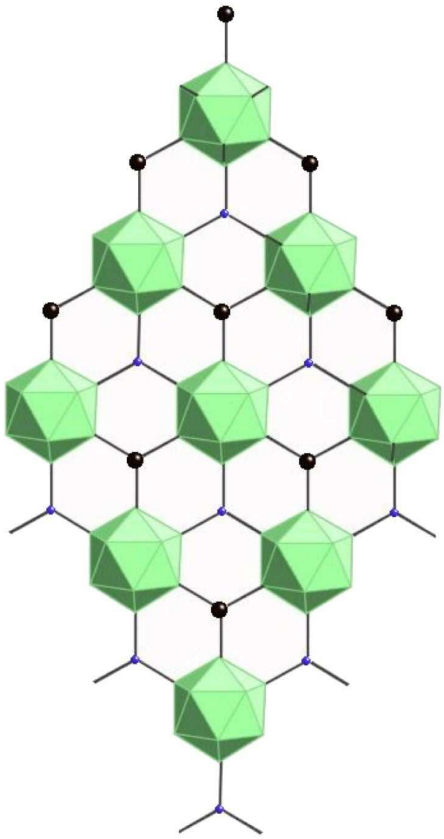

Figure 13. B_{12} icosahedron network bridged by nitrogen (blue) and carbon (black) atoms.

in Appendix IVb.

Same metals, Y, Ho, Er, Tm and Lu, also form $REB_{28.5}C_4$ which has a trigonal crystal structure with space group $R\overline{3}m$ (No. 166) [27]. Lattice constants of the representative compound $YB_{28.5}C_4$ are $a = b = 0.56457(9)$ nm and $c = 5.68873(13)$ nm and there are six formula units in the unit cell. Structure data of $YB_{28.5}C_4$ are summarized in Appendix IVc.

6. $\mathbf{RE}_x\mathbf{B}_{12}\mathbf{C}_{0.33}\mathbf{Si}_{3.0}$

Initially we have reported this group as ternary RE-B-Si compounds [29, 30, 31], but later included carbon for better structure description [32]; thus, they are now understood as quaternary RE-B-C-Si compounds. $RE_xB_{12}C_{0.33}Si_{3.0}$ (RE=Y and Gd-Lu) have a unique crystal structure with two units - a cluster of B_{12} icosahedra and a Si_8 ethane-like cluster - and one bonding configuration $(B_{12})_3{\equiv}$Si-C$\equiv(B_{12})_3$. Here, we consider $Y_xB_{12}C_{0.33}Si_{3.0}$ (x=0.68) as a representative compound. It has a trigonal crystal structure with space group $R\overline{3}m$ (No. 166) and lattice constants $a = b = 1.00841(4)$ nm, $c = 1.64714(5)$ nm, $\alpha = \beta = 90°$ and $\gamma = 120°$.

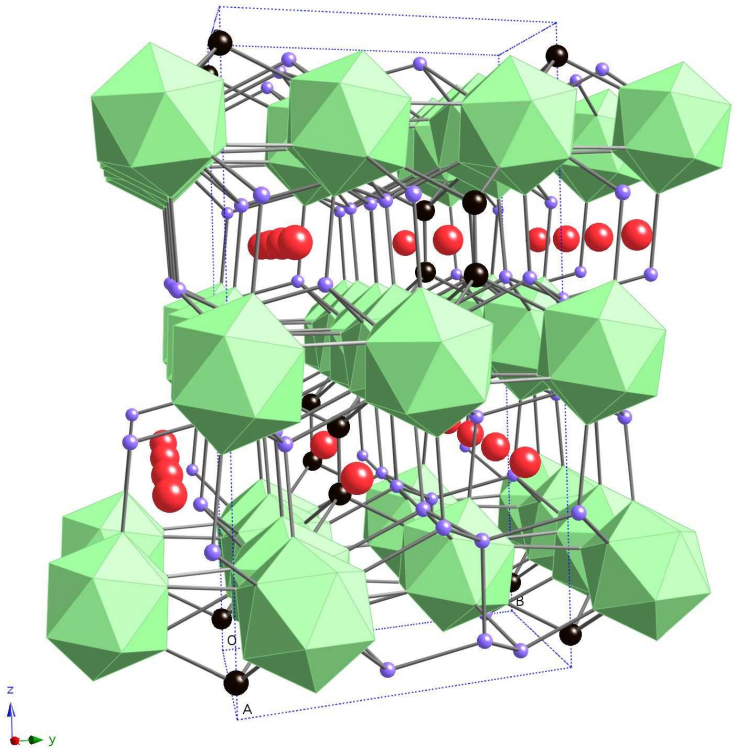

Figure 14. Crystal structure of $RE_xB_{12}C_{0.33}Si_{3.0}$ (RE=Y or Dy) viewed along the direction close to [100]. Red, black and blue spheres correspond to Y or Dy, C and Si atoms, respectively. Vacancies at the Y or Dy site are ignored. Green polyhedra indicate the B_{12} icosahedra.

There are eight atomic sites in the unit cell: one yttrium Y, four boron B1-B4, one carbon C3 and three silicon sites Si1-Si3. Atomic coordinates, site occupancy and isotropic displacement factors are listed in Appendix Va. Sixty eight percent of the Y sites are randomly occupied and remaining Y sites are vacant. All boron sites and Si1 and Si2 sites are fully occupied. C3 and Si3 sites can be occupied by either carbon or silicon atoms (mixed occupancy) with a probability of about 50%. Their separation is only 0.413 Å, and thus either C3 or Si3 site, but not both, are occupied. These cites form a Si-C pair, but not a Si-Si or C-C pair. The distances between the C3 and Si3 sites and the surrounding sites for $Y_xB_{12}C_{0.33}Si_{3.0}$ are summarized in Appendix Vb and the overall crystal structure is shown in figure 14.

The crystal has layered structure. Figure 15 shows a network of boron icosahedra that spreads parallel to the (001) plane, connecting with four neighbors through B1-

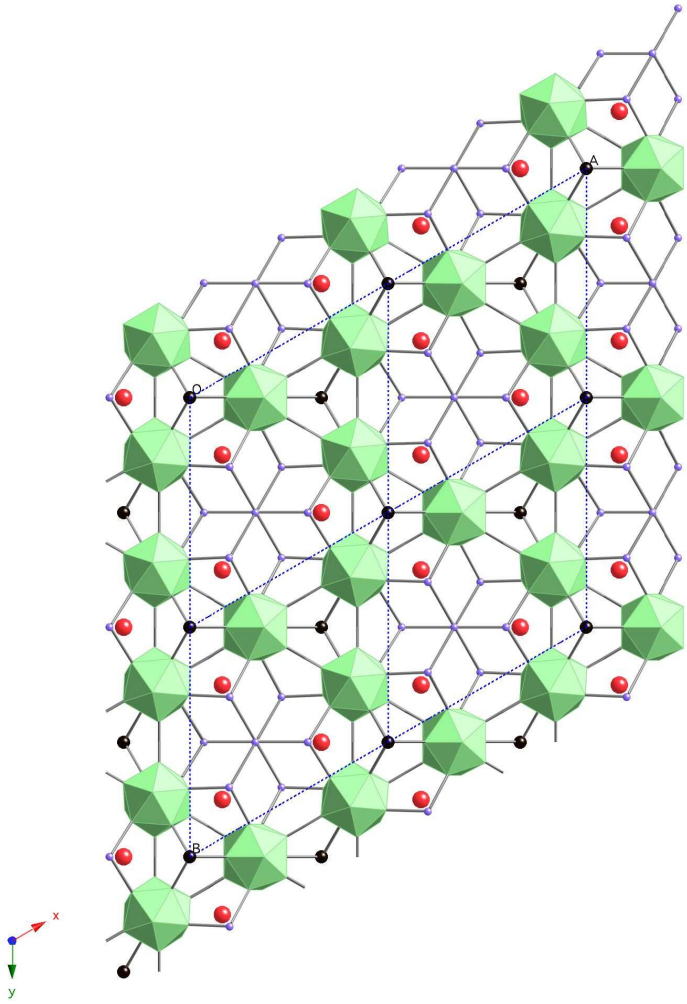

Figure 15. A network of boron icosahedra lying in the (001) plane. Black, blue and red spheres correspond to C, Si and Y atoms, respectively.

B1 bonds. The C3 and Si3 site atoms strengthen the network by bridging the boron icosahedra. Contrary to other boron-rich icosahedral compounds, the boron icosahedra from different layers are not directly bonded. The icosahedra within one layer are linked through Si_8 ethane like clusters with $(B_{12})_3$≡Si-C≡$(B_{12})_3$ bonds, as shown in figures 16(a) and (b).

Salvador *et al* [33] reported an isotypic terbium compound $Tb_{3-x}C_2Si_8(B_{12})_3$. Most parts of the crystal structure are the same as those described above; however, Salvador *et al* deduced the bonding configuration of $(B_{12})_3$≡C-C≡$(B_{12})_3$ instead of $(B_{12})_3$≡Si-C≡$(B_{12})_3$. They intentionally added carbon to grow single crystals whereas our samples were accidentally contaminated by carbon during crystal growth. Thus, Salvador's samples could have higher carbon concentration than ours. Existence of both bonding schemes of $(B_{12})_3$≡Si-C≡$(B_{12})_3$ and $(B_{12})_3$≡C-C≡$(B_{12})_3$ suggests a solid-solubility region of carbon at the site from 50 to 100%. On the other hand, $(B_{12})_3$≡Si-Si≡$(B_{12})_3$ bonding scheme is unlikely because of too short Si-Si distance, suggesting

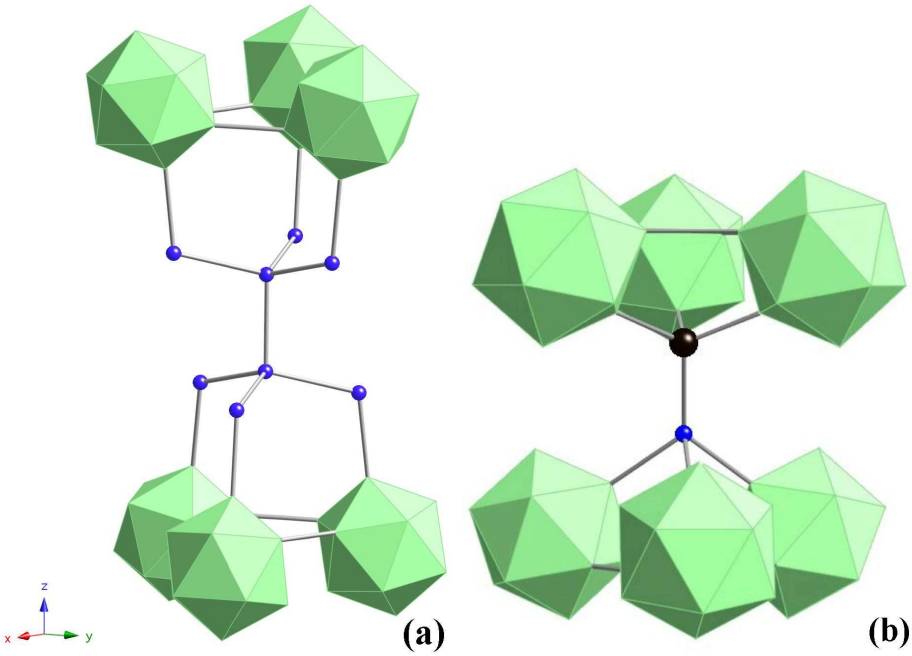

Figure 16. (a) Si_8 ethane-like cluster connects layers of boron icosahedra; a layer of boron icosahedra that lies at the same level as the Si_8 cluster is not shown. (b) bonding configuration $(B_{12})_3$≡Si-C≡$(B_{12})_3$

.

that the minimum carbon occupancy at the site is 50%. Some B atoms may replace C atoms at the C3 site, as previously assigned to the B site [31]. However, the carbon occupation is more likely because the site is tetrahedrally coordinated whereas the B occupation of the site needs an extra electron to complete tetrahedral bonding. Thus, carbon is indispensable for this group of compounds.

7. Scandium compounds

Scandium has the smallest atomic and ionic (3+) radii (1.62 and 0.885 Å, respectively) among the metals considered in this review. The second smallest values are those of lutetium (1.74 and 1.001 Å). Scandium forms several icosahedron-based borides which are not found for other rare-earth elements; however, most of them are ternary Sc-B-C compounds. There are many boron-rich phases in the boron-rich corner of Sc-B-C phase diagram, as shown in figure 17. A slight variation of the composition can produce ScB_{19}, $ScB_{17}C_{0.25}$, $ScB_{15}C_{0.8}$ and $ScB_{15}C_{1.6}$; their crystal structures are unusual and very different among each other.

7.1. $ScB_{19+x}Si_y$

$ScB_{19+x}Si_y$ has a tetragonal crystal structure with space group $P41212$ (No. 92) or $P43212$ and lattice constants of a, $b = 1.03081(2)$ and $c = 1.42589(3)$ nm; it is basically

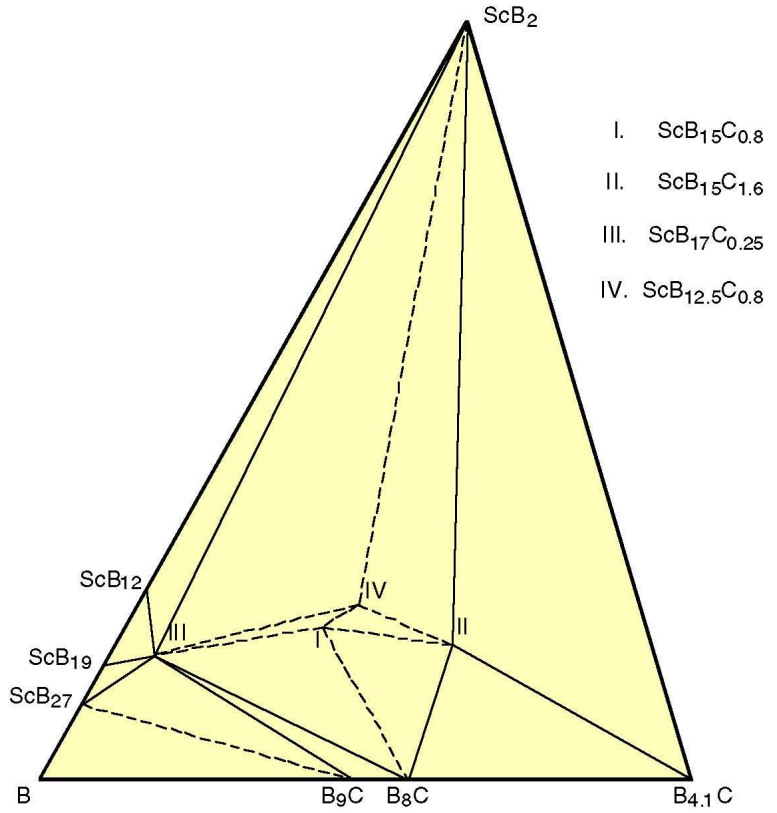

Figure 17. The boron-rich corner of Sc-B-C phase diagram.

isotypic to the α-AlB_{12} structure type [34]. There are 28 atomic sites in the unit cell, which are assigned to 3 scandium atoms, 24 boron atoms and one silicon atom. Atomic coordinates, site occupancies and isotropic displacement factors are listed in Appendix VI.

The boron framework of $ScB_{19+x}Si_y$ is based on one B_{12} icosahedron and one B_{22} unit. This unit can be observed in β-tetragonal boron [35] and is a modification of the B_{20} unit of α-AlB_{12} [36] (or B_{19} unit in the earlier paper [37, 38]). The B_{20} unit is a twinned icosahedron made from B13 to B22 sites with two vacant sites and one B atom (B23) bridging both sides of the unit. The twinned icosahedron is shown in figure 18(a). B23 was treated as an isolated atom in the earlier discussion of the α-AlB_{12} crystal structure [37, 38]. B23 is bonded to each twinned icosahedra through B18 and to another icosahedron through B5 site. If the twinned icosahedra were independent without twinning then B23 would be a bridge site linking three icosahedra. However, because of twinning, B23 shifts closer to the twinned icosahedra than another icosahedron; thus recently, B23 has been treated as a member of the twinned icosahedra. In $ScB_{19+x}Si_y$, the two B24 sites which correspond to the vacant sites in the B_{20} unit are partially occupied; thus, the unit should be referred to as a B_{22} cluster which is occupied by about 20.6 boron atoms. Scandium atoms occupy 3 of 5 Al sites of α-AlB_{12}, that is Sc1, Sc2 and Sc3 correspond to Al4, Al1 and Al2 sites of α-AlB_{12}, respectively. The

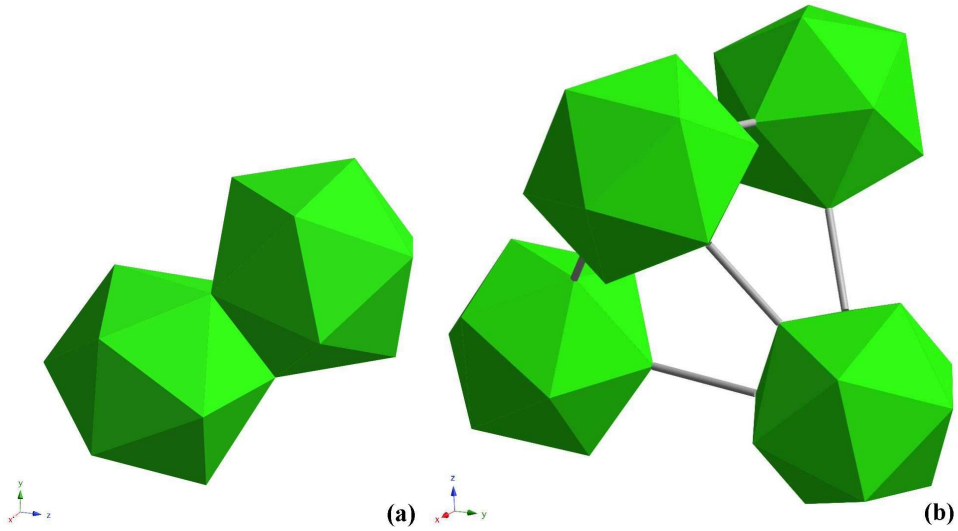

Figure 18. (a) Twinned B_{22} icosahedra, (b) boron supertetrahedron constructed by 4 icosahedra.

Al3 and Al5 sites are empty for $ScB_{19+x}Si_y$. Si site links two B_{22} units. This phase can also exist without Si [39].

Figure 19(a) shows the network of boron icosahedra in the boron framework of $ScB_{19+x}Si_y$. In this network, 4 icosahedra form a supertetrahedron (figure 18(b)); its one edge is parallel to the *a*-axis, and the icosahedra on this edge form a chain along the *a*-axis. The opposite edge of the supertetrahedron is parallel to the *b*-axis and the icosahedra on this edge form a chain along the *b*-axis. As shown in figure 19, there are wide tunnels surrounded by the icosahedron arrangement along the *a*- and *b*-axes. The tunnels are filled by the B_{22} units which strongly bond to the surrounding icosahedra; the connection of the B_{22} units is helical and it runs along the *c*-axis as shown in figure 19(b). Scandium atoms occupy the voids in the boron network as shown in figure 19(c), and the Si atoms bridge the B_{22} units.

7.2. $ScB_{17}C_{0.25}$

Very small amount of carbon could stabilize "$ScB_{17}C_{0.25}$" [40]. This compound has a broad homogeneity region, namely $ScB_{16.5+x}C_{0.2+y}$ with $x \leq 2.2$ and $y \leq 0.44$. $ScB_{17}C_{0.25}$ has a hexagonal crystal structure with space group *P6mmm* (No. 199) and lattice constants *a*, $b = 1.45501(15)$ nm and $c = 0.84543(16)$ nm [41].

There are 19 atomic sites in the unit cell, which are assigned to one scandium site Sc, 14 boron sites B1-B14 having 100% occupancy, two boron-carbon mixed-occupancy sites B/C15 and B/C16, and two partial-occupancy boron sites B17 and B18. Atomic coordinates, site occupancies and isotropic displacement factors are listed in Appendix VII. Although a very small amount of carbon (less than 2 wt%!) plays an important role in the phase stability, carbon does not have its own sites but is diluted over two interstitial sites B/C15 and B/C16.

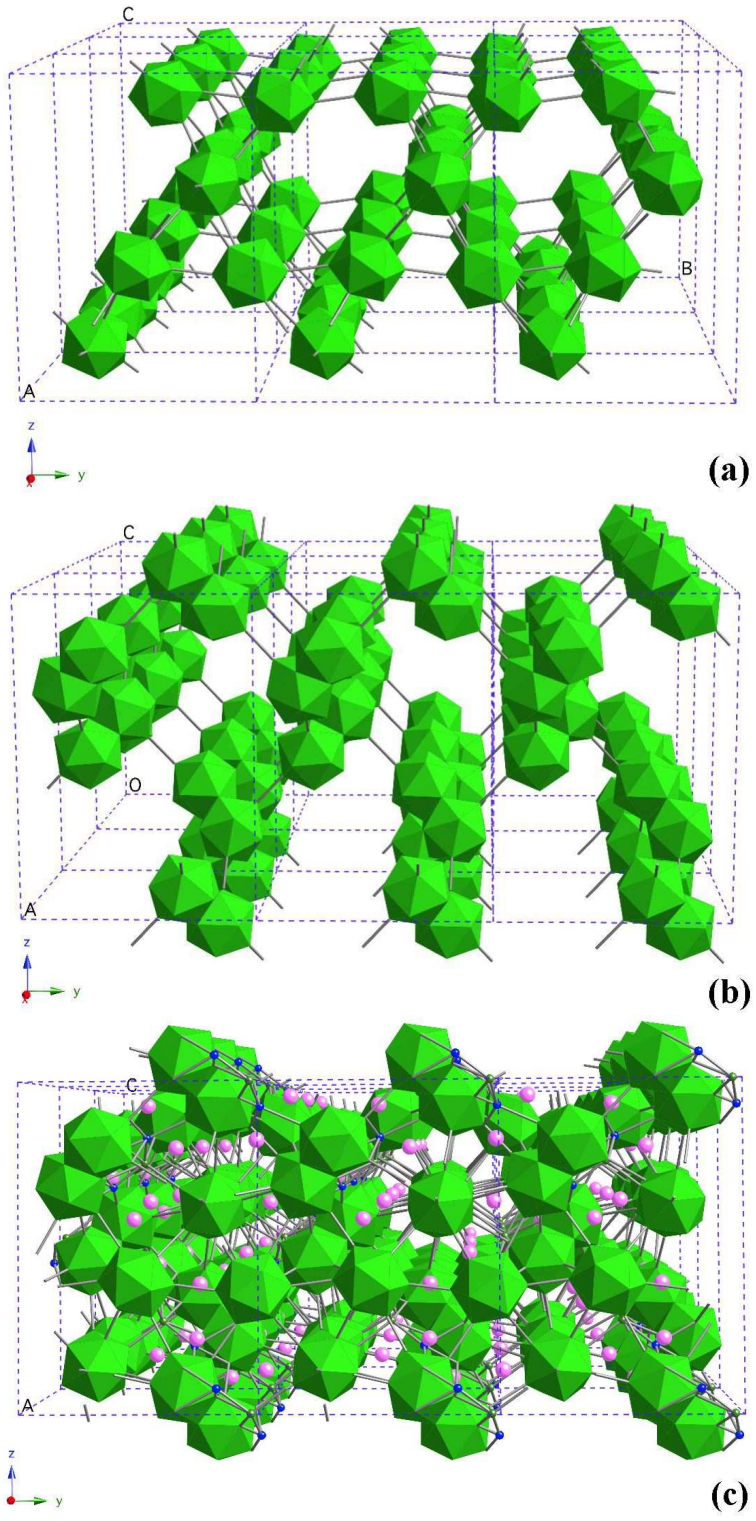

Figure 19. (a) Network of boron icosahedra, (b) B_{22} unit network and (c) overall crystal structure of $ScB_{19+x}Si_y$; pink and blue spheres indicate scandium and silicon atoms, respectively.

There are two inequivalent B_{12} icosahedra, I1 and I2, which are constructed by the B1-B5 and B8-B12 sites, respectively. A "tube" structure is another characteristic structure unit of $ScB_{17}C_{0.25}$ which extends along the *c*-axis. It consists of B13, B14, B17 and B18 sites where B13 and B14 form 6-membered rings. B17 and B18 sites also form 6-membered rings; however, their mutual distances (0.985 Åfor B17 and 0.955 Åfor B18) are too short for a simultaneous occupation of the neighboring sites. Therefore, boron atoms occupy 2nd neighbor site forming a triangle. The occupancies of B17 and B18 sites should be 50%, the structure analysis suggests larger values. The crystal structure viewed along the *a*-axis is shown in figure 20, which suggests that the $ScB_{17}C_{0.25}$ is a layered material. Two layers, respectively constructed by the icosahedra I1 and I2, alternatively stack along the *c*-axis. However, the $ScB_{17}C_{0.25}$ crystal is not layered. For example, in an arc-melting experiment, $ScB_{17}C_{0.25}$ needle crystals violently grow along the *c*-axis - this never happens in layered compounds. The crystal structure viewed along the *c*-axis is shown in figure 21(a). The icosahedra I1 and I2 form a ring centered by the "tube" shown in figure 21(b), which probably governs the properties of the $ScB_{17}C_{0.25}$ crystal. B/C15 and B/C16 mixed-occupancy sites interconnect the rings. A structural similarity can be seen between $ScB_{17}C_{0.25}$ and BeB_3 [1].

Figures 22(a) and (b) present HRTEM lattice images and electron diffraction patterns taken along the [0001] and [11$\bar{2}$0] crystalline directions, respectively. The HRTEM lattice image of figure 22(a) reproduces well the (*a*, *b*) plane of the crystal structure shown in figure 21(a), with the clearly visible rings membered by icosahedra I1 and I2 and centered by the "tube". Meanwhile, figure 22(b) proves that $ScB_{17}C_{0.25}$ does not have layered character but its *c*-axis direction is built up by the ring-like structure and the "tube" structure.

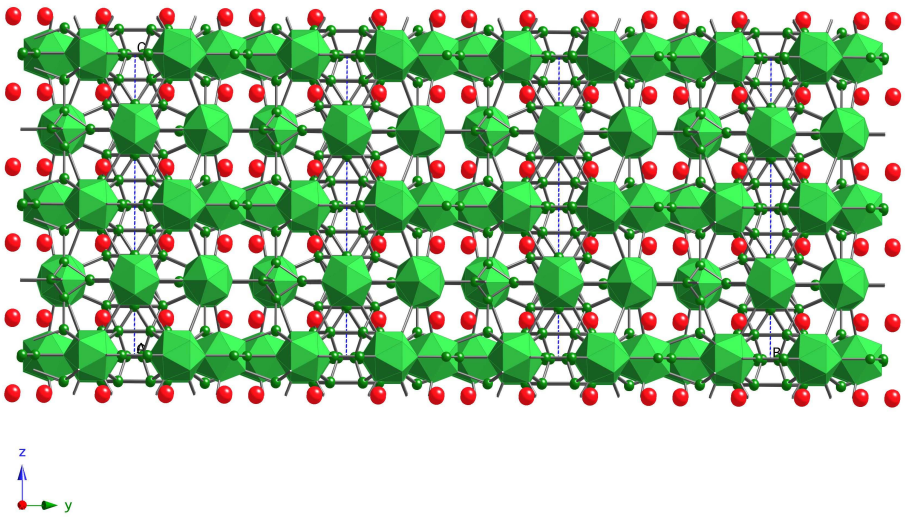

Figure 20. $ScB_{17}C_{0.25}$ crystal structure viewed along the *a*-axis. Icosahedron layers alternatively stack along the *c*-axis in the order I1-I2-I1-I2-I1.

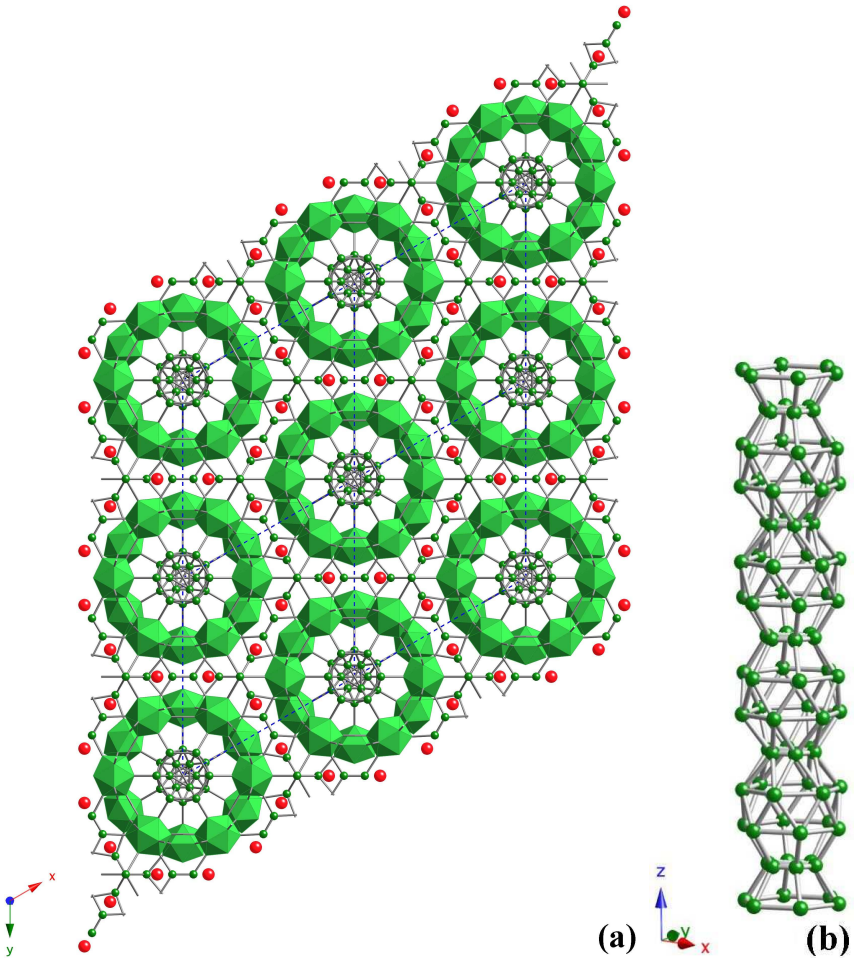

Figure 21. (a) $ScB_{17}C_{0.25}$ crystal structure viewed along the *c*-axis. Icosahedra I1 and I2 form a ring centered by a "tube". (b) The "tube" structure that runs along the *c*-axis. Partial occupancies of B17 and B18 are ignored.

7.3. $Sc_{0.83-x}B_{10.0-y}C_{0.17+y}Si_{0.083-z}$ ($x = 0.030$, $y = 0.36$ and $z = 0.026$)

$Sc_{0.83-x}B_{10.0-y}C_{0.17+y}Si_{0.083-z}$ has a cubic crystal structure with space group $F\overline{4}3m$ (No. 216) and lattice constant $a = 2.03085(5)$ nm [42]. This compound was initially assigned as $ScB_{15}C_{0.8}$ (phase I in the Sc-B-C phase diagram of figure 17). A small amount of Si was added into the floating zone crystal growth and thus this phase is a quaternary compound. Its cubic structure is new and has 26 cites in the unit cell: three Sc sites, two Si sites, one C site and 20 B sites; 4 out of 20 B sites are boron-carbon mixed-occupancy sites. Atomic coordinates, site occupancies and isotropic displacement factors are listed in Appendix VIII.

In the unit cell, there are three independent icosahedra, I1, I2 and I3, and a B_{10} polyhedron which are formed by the B1-B4, B5-B8, B9-B13 and B14-B17 sites, respectively. The B_{10} polyhedron has not been observed previously and it is shown in figure 23.

The icosahedron I2 has a boron-carbon mixed-occupancy site B,C6 whose

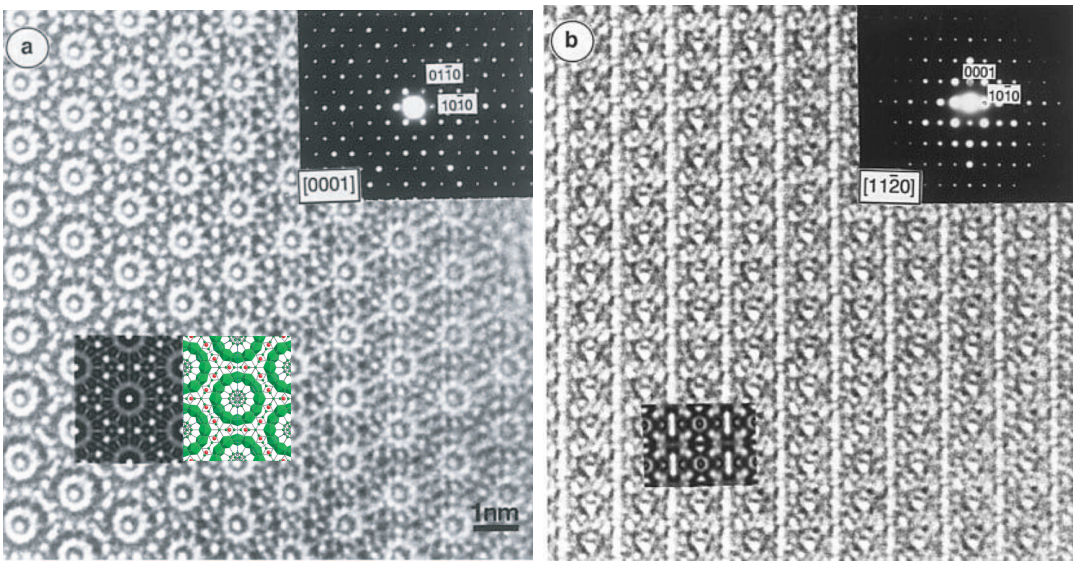

Figure 22. HRTEM lattice images and electron diffraction patterns (top-right insets) taken along the (a) [0001] and (b) [11$\bar{2}$0] directions. Image simulations are added in the bottom-left insets, and the corresponding crystal structure is also added in (a).

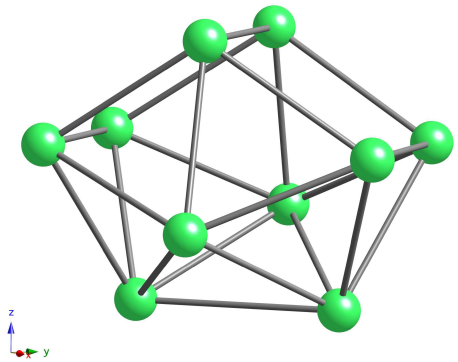

Figure 23. B_{10} polyhedron in the $Sc_{0.83-x}B_{10.0-y}C_{0.17+y}Si_{0.083-z}$ crystal structure.

occupancy is B/C=0.58/0.42. Remaining 3 boron-carbon mixed occupancy sites are bridge sites; C and Si sites are also bridge sites.

More than 1000 atoms are available in the unit cell. It is not so easy to build the structure using only the icosahedra I1-I3 and the B_{10} polyhedron, and therefore we employed larger structure units such as two supertetrahedra T(1) and T(2) and one superoctahedron O(1). As shown in figure 24(a), T(1) consists of 4 icosahedra I(1) which have no direct bonding but are bridged by four B,C20 atoms. These atoms also form tetrahedron centered by Si2 sites. The supertetrahedron T(2) that consists of 4 icosahedra I(2) is the same as shown in figure 18(b); its mixed occupancy sites B,C6 directly bond with each other. The superoctahedron O(1) consists of 6 icosahedra I(3) and bridge sites B,C18, C1 and Si1; here Si1 and C1 exhibit a tetrahedral arrangement at the center of O(1). Interestingly, the B_{10} polyhedra also arrange octahedrally, without

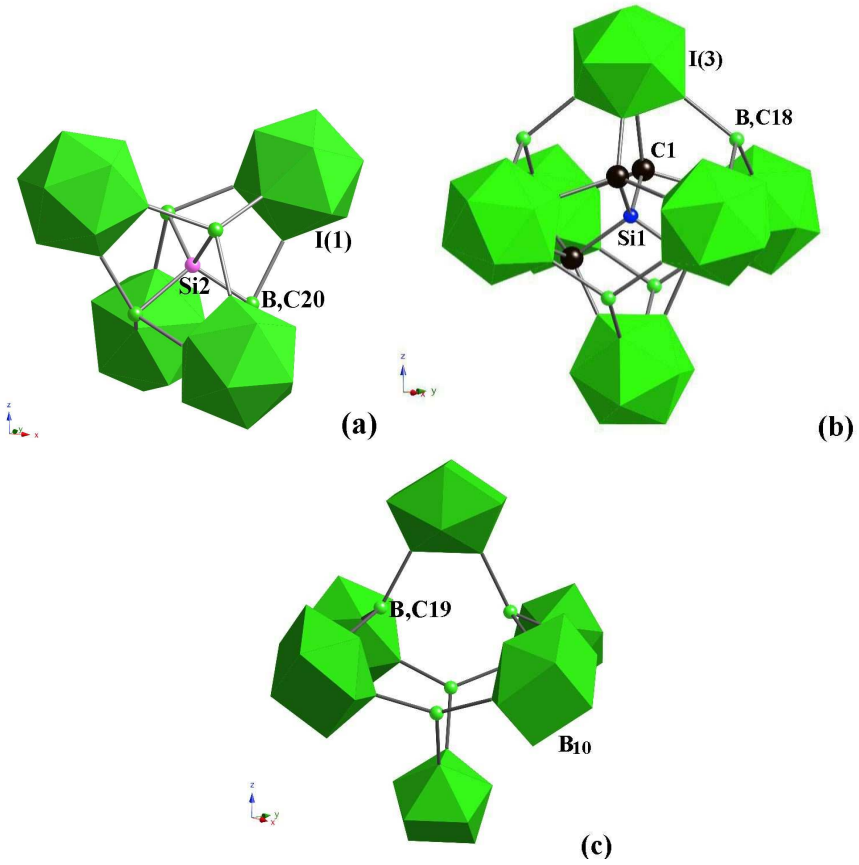

Figure 24. (a) Supertetrahedron T(1), (b) superoctahedron O(1) and (c) octahedral arrangement of the B_{10} polyhedra in the $Sc_{0.83-x}B_{10.0-y}C_{0.17+y}Si_{0.083-z}$ crystal structure.

the central atom, as shown in figure 24(c) where the B,C19 atoms bridge the B_{10} polyhedra to form the octahedral supercluster of the B_{10} polyhedra.

Using these superpolyhedra, the crystal structure of $Sc_{0.83-x}B_{10.0-y}C_{0.17+y}Si_{0.083-z}$ can be described as shown in figure 25. Owing to the crystal symmetry, the tetrahedral coordination between these super structure units is again a key factor. The supertetrahedron T(1) lies at the body center and at the edge center of the unit cell. The superoctahedra O(1) locate at the body center (0.25, 0.25, 0.25) of the quarter of the unit cell. They coordinate tetrahedrally around T(1) forming a giant tetrahedron. The supertetrahedra T(2) are located at the symmetry-related positions (0.25, 0.25, 0.75); they also form a giant tetrahedron surrounding T(1). Edges of both giant tetrahedra orthogonally cross each other at their centers; at those edge centers, each B_{10} polyhedron bridges all the super-structure clusters T(1), T(2) and O(1). The superoctahedron built of B_{10} polyhedra is located at each cubic face center.

Scandium atoms reside in the voids of the boron framework. Four Sc1 atoms form a tetrahedral arrangement inside the B_{10} polyhedron-based superoctahedron. Sc2 atoms sit between the B_{10} polyhedron-based superoctahedron and the O(1) superoctahedron.

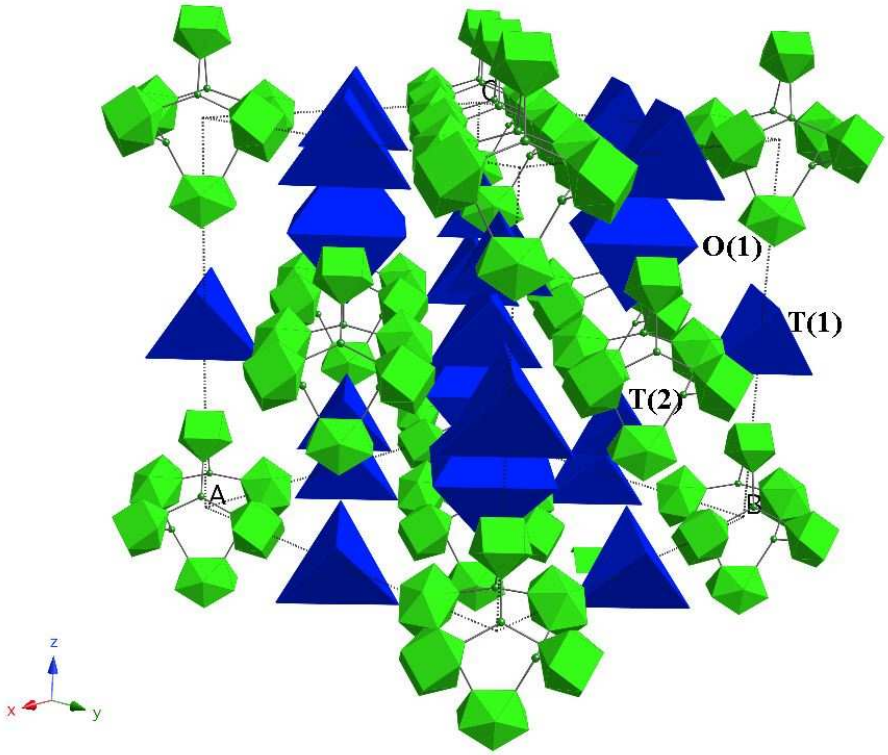

Figure 25. Boron framework structure of $Sc_{0.83-x}B_{10.0-y}C_{0.17+y}Si_{0.083-z}$ depicted by supertetrahedra T(1) and T(2), superoctahedron O(1) and the superoctahedron based on B_{10} polyhedron. Vertexes of each superpolyhedron are adjusted to the center of the constituent icosahedra, thus the real volumes of these superpolyhedra are larger than appear in the picture.

Three Sc3 atoms form a triangle and are surrounded by three B_{10} polyhedra, a supertetrahedron T(1) and a superoctahedron O(1).

7.4. $ScB_{14-x}C_x$ (x = 1.1) and $ScB_{15}C_{1.6}$

$ScB_{14-x}C_x$ has an orthorhombic crystal structure with space group *Imma* (No. 74) and lattice constants of $a = 0.56829(2)$, $b = 0.80375(3)$ and $c = 1.00488(4)$ nm. The crystal structure of $ScB_{14-x}C_x$ is isotypic to that of $MgAlB_{14}$ where Sc occupies the Mg site, the Al site is empty and the boron bridge site is a B/C mixed-occupancy site with the occupancy of B/C = 0.45/0.55 [43]. The occupancy of the Sc site in a flux-grown single crystal is 0.964(4), i.e. almost 1. Solid-state powder-reaction growth resulted in lower Sc site occupancy and in the resulting chemical composition $ScB_{15}C_{1.6}$ [40]. The B-C bonding distance 0.1796(3) nm between the B/C bridge sites is rather long as compared with that (0.15 $\sim$ 0.16 nm) of an ordinary B-C covalent bond, that suggests weak bonding between the B/C bridge sites.

7.5. $Sc_{4.5-x}B_{57-y+z}C_{3.5-z}$ (x =0.27, y = 1.1, z = 0.2)

$Sc_{4.5-x}B_{57-y+z}C_{3.5-z}$ has an orthorhombic crystal structure with space group *Pbam* (No. 55) and lattice constants of $a = 1.73040(6)$, $b = 1.60738(6)$ and $c = 1.44829(6)$ nm [44]. This phase is indicated as $ScB_{12.5}C_{0.8}$ (phase IV) in the phase diagram of figure 17. This orthorhombic structure is new and has 78 atomic positions in the unit cell: seven partially occupied Sc, four C, 66 B sites with three partially occupied sites and one B/C mixed-occupancy site. Atomic coordinates, site occupancies and isotropic displacement factors are listed in Appendix IX.

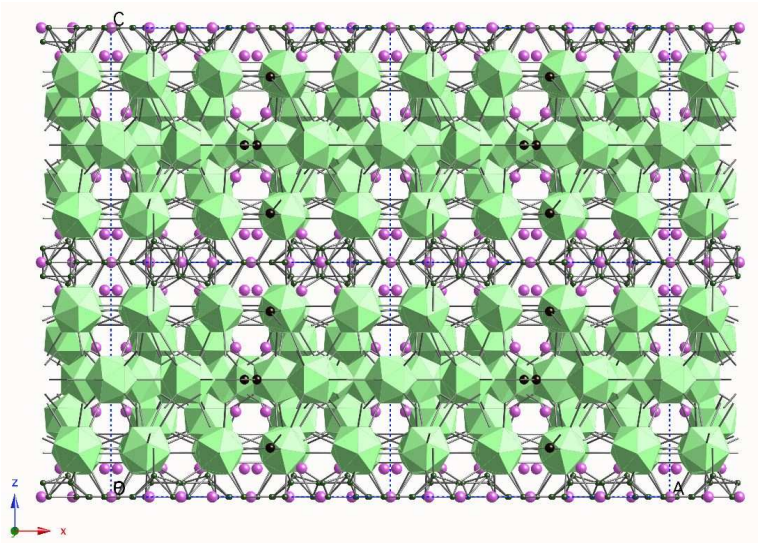

Figure 26. $Sc_{4.5-x}B_{57-y+z}C_{3.5-z}$ crystal structure viewed along the [010] direction; 2.5 and 2 unit-cell sizes are depicted along the x-axis and z-axis, respectively.

More than 500 atoms are available in the unit cell. In the crystal structure, there are six structurally independent icosahedra I1-I6, which are constructed from B1-B12, B13-B24, B25-B32, C33-B40, B41-B44 and B45-B56 sites, respectively; B57-B62 sites form a B_8 polyhedron. The $Sc_{4.5-x}B_{57-y+z}C_{3.5-z}$ crystal structure is layered, as shown in figure 26. We have previously described this structure in terms of two kinds of boron icosahedron layers, L1 and L2. L1 consists of the icosahedra I3, I4 and I5 and the C65 "dimer", and L2 consists of the icosahedra I2 and I6. I1 is sandwiched by L1 and L2 and the B_8 polyhedron is sandwiched by L2.

Here we present another description based on the same $B_{12}(B_{12})_{12}$ supericosahedron as that of YB_{66}. In the YB_{66} crystal structure, the supericosahedra form 3-dimensional boron framework as shown in figure 5. In this framework, the neighboring supericosahedra are rotated 90° with respect to each other. On the contrary, in $Sc_{4.5-x}B_{57-y+z}C_{3.5-z}$ the supericosahedra form a 2-dimensional network where the 90° rotation relation is broken because of the orthorhombic symmetry. The planar projections of the supericosahedron connection in $Sc_{4.5-x}B_{57-y+z}C_{3.5-z}$ and YB_{66} are shown in figures 27(a) and (b), respectively. In the YB_{66} crystal structure,

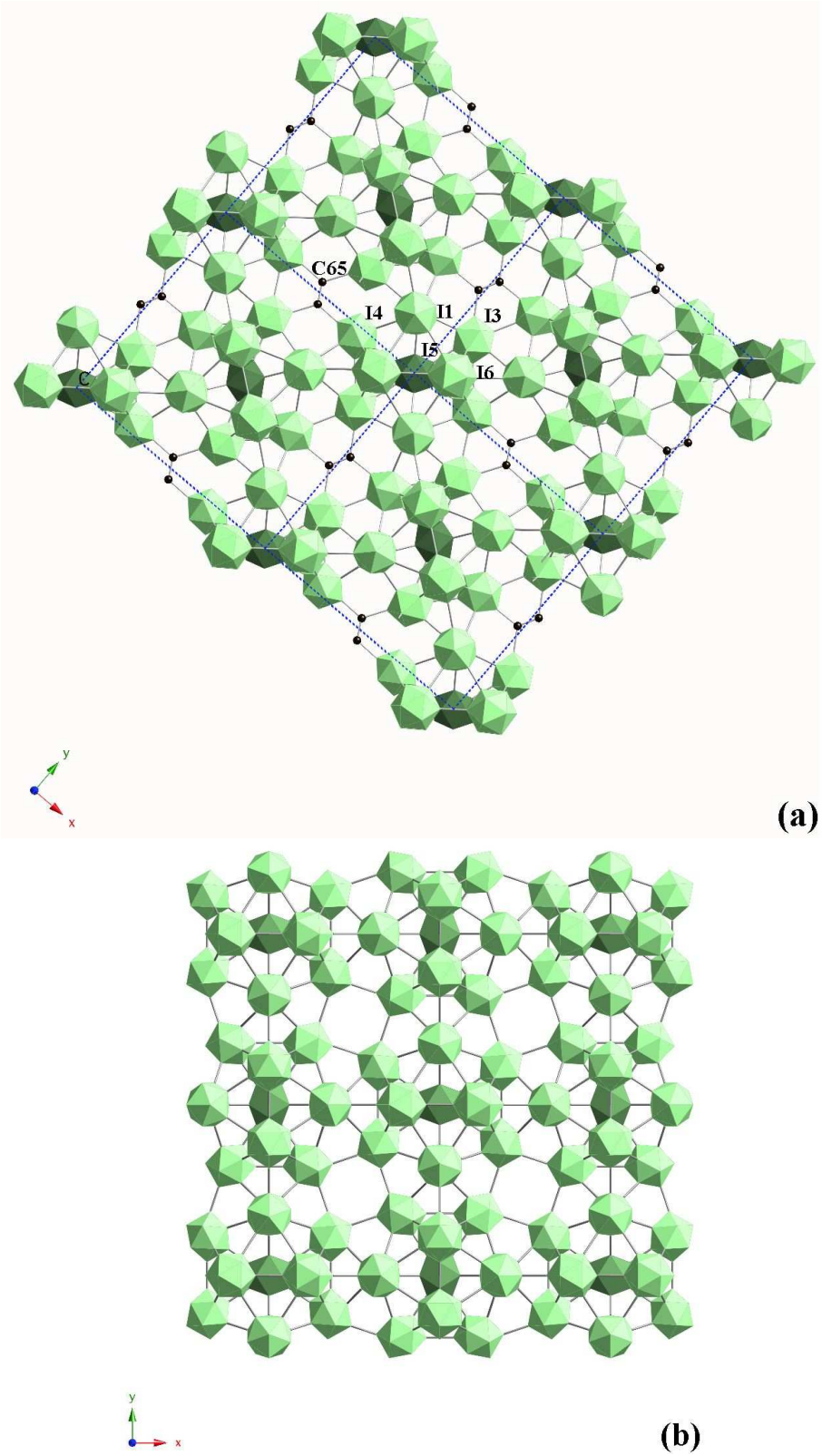

Figure 27. Two-dimensional presentation of supericosahedron connection in (a) $Sc_{4.5-x}B_{57-y+z}C_{3.5-z}$ and (b) YB_{66}. The central icosahedra of the supericosahedron are dark green.

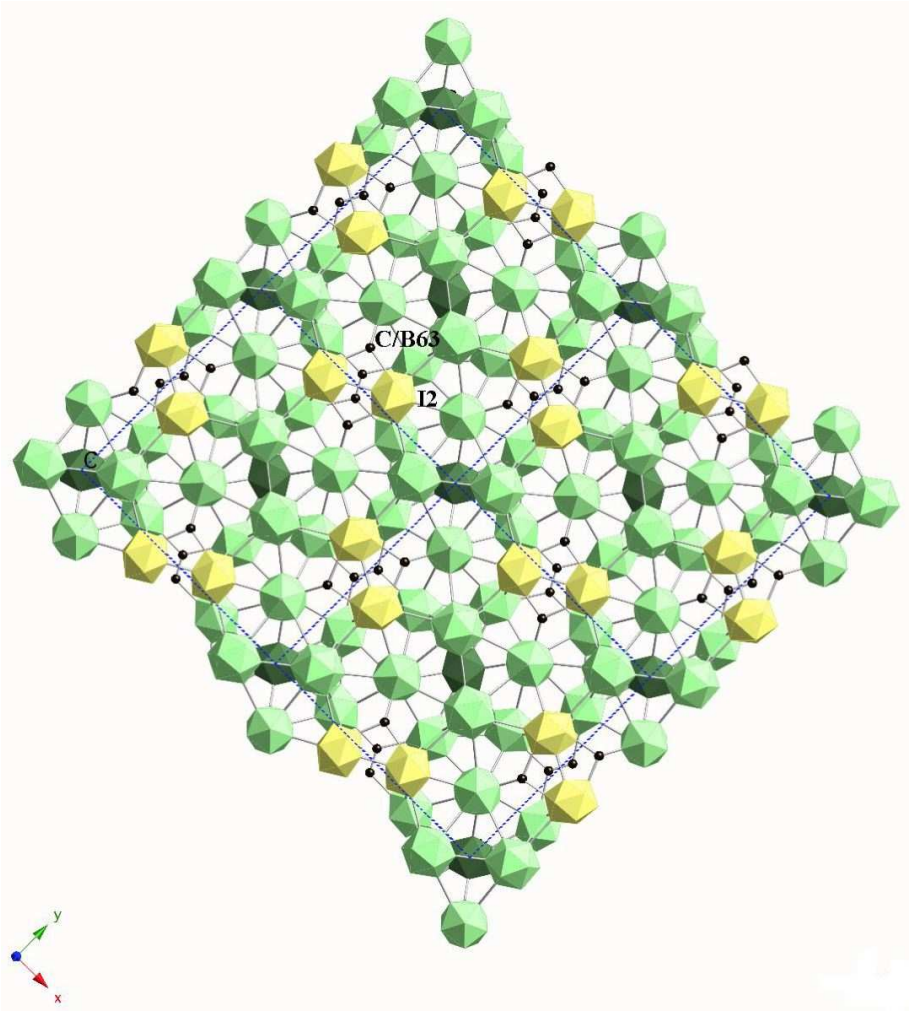

Figure 28. Locations of the I2 icosahedron (yellow) in the 2-dimensional supericosahedron framework of $Sc_{4.5-x}B_{57-y+z}C_{3.5-z}$.

the neighboring 2-dimensional supericosahedron connections are out-of-phase for the rotational relation of the supericosahedron. This allows 3-dimensional stacking of the 2-dimensional supericosahedron connection while maintaining the cubic symmetry.

The B_{80} boron cluster occupies the large space between four supericosahedra as described in the REB_{66} section. On the other hand, the 2-dimensional supericosahedron networks in the $Sc_{4.5-x}B_{57-y+z}C_{3.5-z}$ crystal structure stack in-phase along the z-axis. Instead of the B_{80} cluster, a pair of the I2 icosahedra fills the open space staying within the supericosahedron network, as shown in figure 28 where the icosahedron I2 is colored in yellow.

All Sc atoms except for Sc3 reside in large spaces between the supericosahedron networks, and the Sc3 atom occupies a void in the network as shown in figure 26. Because of small size of Sc atom, the occupancies of Sc1-Sc5 site exceed 95%, and those of Sc6 and Sc7 sites are approximately 90 and 61%, respectively, as listed in appendix IX.

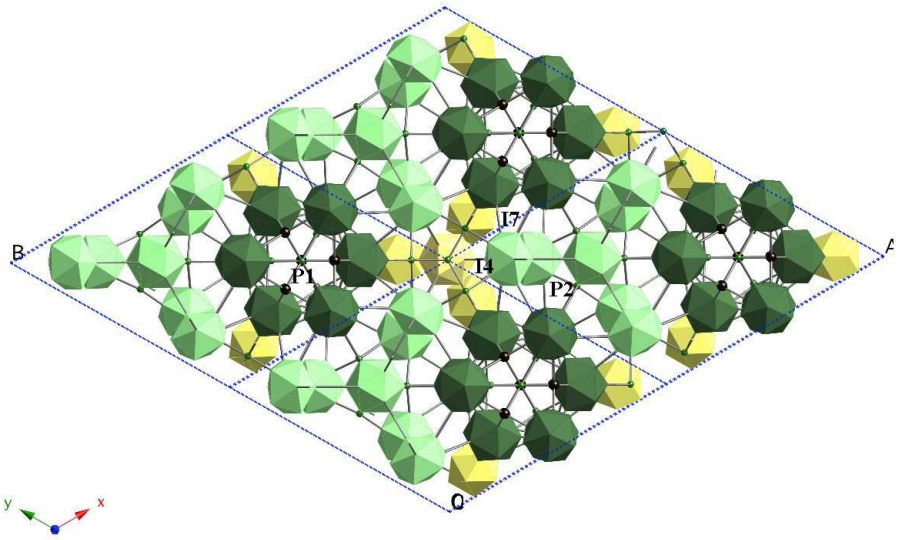

Figure 29. Boron framework structure of $Sc_{3.67-x}B_{41.4-y-z}C_{0.67+z}Si_{0.33-w}$ viewed along the *c*-axis

7.6. $Sc_{3.67-x}B_{41.4-y-z}C_{0.67+z}Si_{0.33-w}$ (x = 0.52, y = 1.42, z = 1.17 and w = 0.02)

$Sc_{3.67-x}B_{41.4-y-z}C_{0.67+z}Si_{0.33-w}$ has a hexagonal crystal structure with space group $P\overline{6}m2$ (No. 187) and lattice constants $a = b = 1.43055(8)$ and $c = 2.37477(13)$ nm [45]. Single crystals of this compound were obtained as an intergrowth phase in the float-zoned single crystal of $Sc_{0.83-x}B_{10.0-y}C_{0.17+y}Si_{0.083-z}$. This phase is not described in the phase diagram (figure 17) because it is a quaternary compound. Its hexagonal structure is a new structure type. There are 79 atomic positions in the unit cell: eight partially occupied Sc sites, 62 B sites, two C sites, two Si sites and six B/C sites. Six B sites have partial occupancy and one of the two Si sites has partial occupancy. Atomic coordinates, site occupancies and isotropic displacement factors are listed in Appendix X.

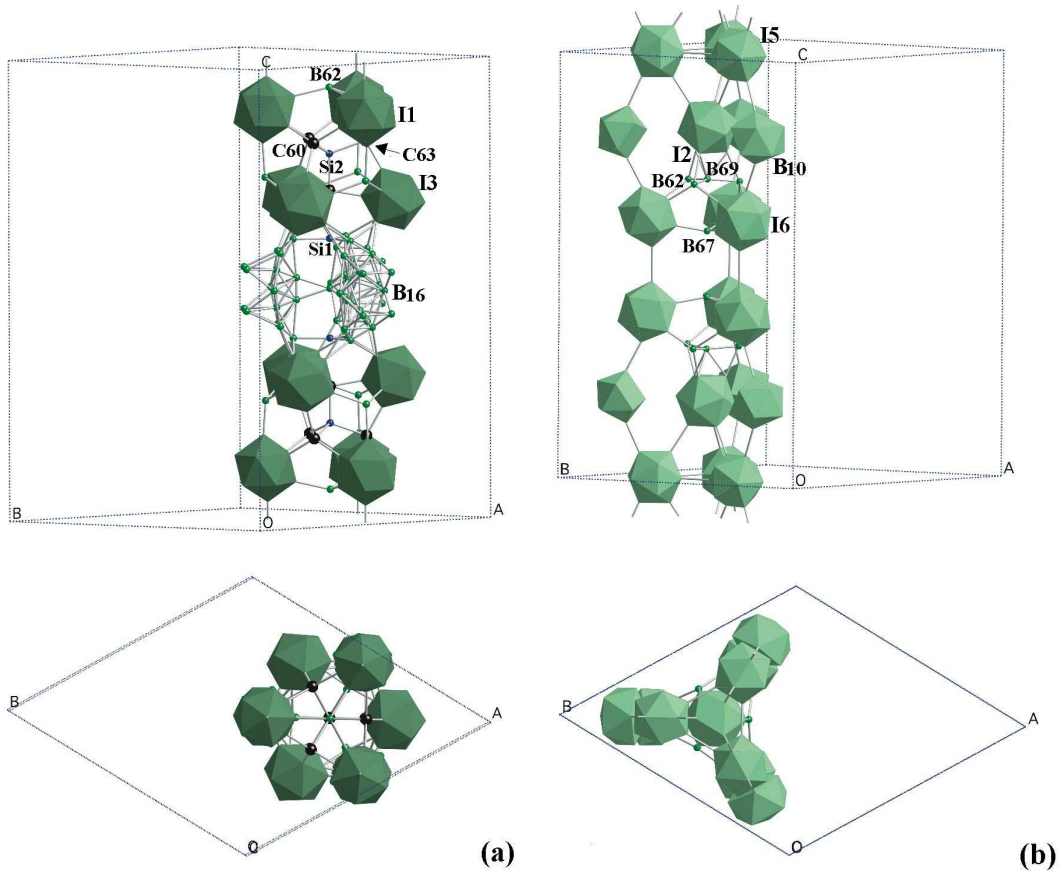

Figure 30. (a) Pillar-like structure unit P1 that consists of icosahedra I1 and I3, irregularly shaped B_{16} polyhedron and other bridge site atoms. (b) Pillar-like structure unit P2 that consists of icosahedra I2, I5 and I6, B_{10} polyhedron and other bridge site atoms.

There are seven structurally independent icosahedra I1-I7 which are formed by B1-B8, B9-B12, B13-B20, B/C21-B24, B/C25-B29, B30-B37 and B/C38-B42 sites, respectively; B43-B46 sites form the B_9 polyhedron and B47-B53 sites construct the B_{10} polyhedron. B54-B59 sites form the irregularly shaped B_{16} polyhedron in which only 10.7 boron atoms are available because most of sites are too close to each other to be occupied simultaneously. Ten bridging sites C60-B69 interconnect polyhedron units or other bridging sites to form a 3D boron framework structure. To describe the crystal structure, we have previously extracted three pillar-like units that extend along the *c*-axis [45]. However, there were some undesired overlaps between those three pillar-like units. Here we define two pillar-like structure units. Figure 29 shows the boron framework structure of $Sc_{3.67-x}B_{41.4-y-z}C_{0.67+z}Si_{0.33-w}$ viewed along the *c*-axis, where the pillar-like units P1 and P2 are colored in dark green and light green, respectively and are bridged by yellow icosahedra I4 and I7.

These pillar-like units P1 and P2 are shown in figures 30(a) and (b), respectively. P1 consists of icosahedra I1 and I3, irregularly shaped B_{16} polyhedron and other bridge site atoms where two supericosahedra can been seen above and below the B_{16} polyhedron. Each supericosahedron is formed by three icosahedra I1 and three icosahedra I3 and is the same as the supericosahedron O(1) shown in figure 24(a).

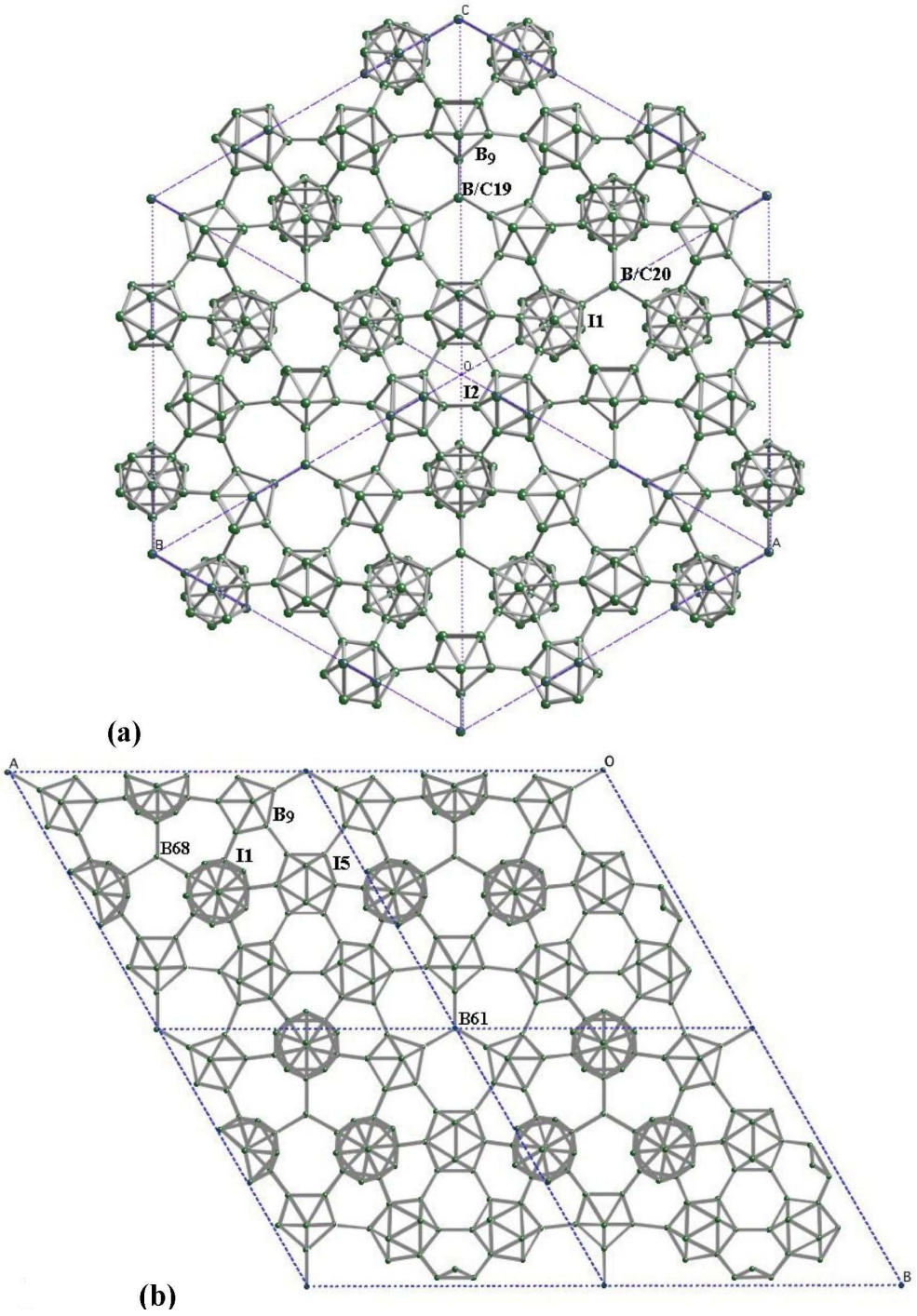

Figure 31. (a) The sliced (111) network structure of the cubic phase, and (b) the (001) boron network layer of the hexagonal phase.

The P2 unit consists of icosahedra I2, I5 and I6, B_{10} polyhedron and other bridge site atoms. Eight Sc sites whose occupancy vary from 0.98 (Sc1) to 0.49 (Sc8) spread over the boron framework.

As described above, this hexagonal phase originates from the cubic phase. Thus we may expect a similar structural element in these phases. There is an obvious relation between the hexagonal *ab*-plane and the cubic (111) plane. Figures 31(a) and (b) show the hexagonal (001) and the cubic (111) planes, respectively. Both network structures are almost the same that allows intergrowth of the hexagonal phase in the cubic phase.

8. Potential applications

As demonstrated in this review, crystal structures of rare-earth boron-rich borides are very diverse. Those borides have interesting physical properties and potential applications in thermoelectric power generation [46]. Thermal conductivity of boron icosahedra based compounds is low because of their complex crystal structures; this property is favored for thermoelectric materials. On the other hand, these compounds exhibit very low (variable-range hopping type) p-type electric conductivity. Increasing the conductivity is a key issue for thermoelectric applications of these borides.

YB_{66} is used as a soft-X-ray monochromator for dispersing 1-2 keV synchrotron radiation at some synchrotron radiation facilities [47]. Contrary to thermoelectric applications, high thermal conductivity is desirable for synchrotron radiation monochromators. YB_{66} exhibits low, amorphous-like thermal conductivity. We have employed transition metal doping to improve thermal conductivity of YB_{66} and increased the thermal conductivity twice in $YNb_{0.3}B_{62}$ as compared to undoped YB_{66} [48].

Very recently, a new structure type of elemental boron has been discovered. Its symmetry is orthorhombic with space group *Pnnm* (No. 58) and lattice constants of $a = 0.50563$, $b = 0.56126$ and $c = 0.6971$ nm [49, 50]. This phase (see figure 32) is produced under high-pressures and at high temperatures; it is quenchable to ambient condition and is the densest among the known boron allotropes. Application of such synthetic methods may increase the variety of rare-earth boron-rich borides and enhance their physical properties and potential applications. Further investigations are required in this direction.

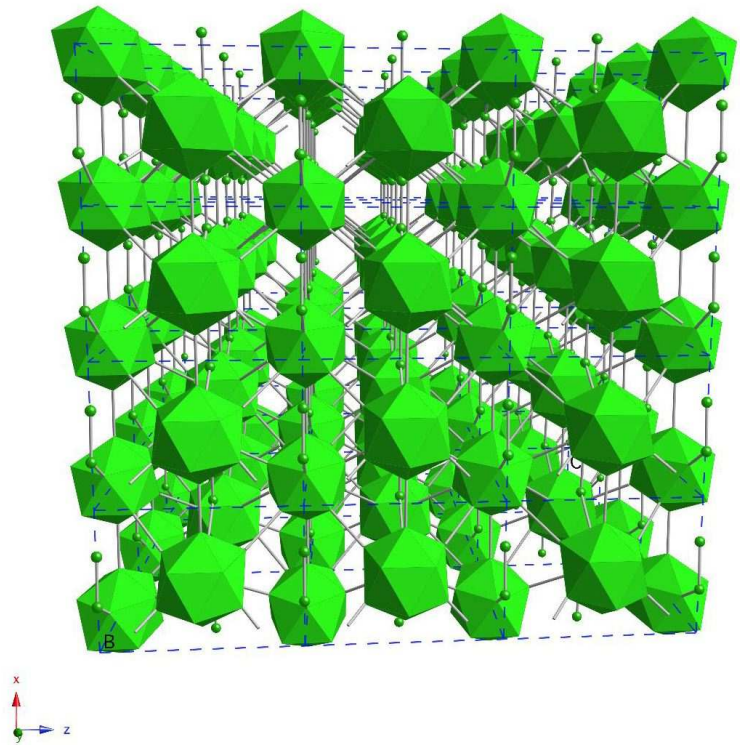

Figure 32. Orthorhombic crystal structure of elemental boron synthesized under high-pressure high-temperature condition. An icosahedron occupies the body center of 4 icosahedra in the orthorhombic unit cell that results in the highest density among the boron allotropes.

References

[1] Chan J Y, Fronczek F R, Young D P, DiTusa J F and Adams P W 2002 *J. Solid State Chem.* **163** 385
[2] Vlasse M, Slack G A, Garbauskas M, Kasper J S and Viala J C 1986 *J. Solid State Chem.* **63** 31
[3] Tanaka T, Okada S and Ishizawa Y 1997 *J. Solid State Chem.* **133** 55
[4] Higashi I, Tanaka T, Kobayashi K, Ishizawa Y and Takami M 1997 *J. Solid State Chem.* **133** 11
[5] Albert B and Hillebrecht H 2009 *Angew. Chem. Int. Ed.* **48** 8668
[6] Werheit H, Filipov V, Kuhlmann U, Schwarz U, Ambrüster M, Leithe-Jasper A, Tanaka T, Higashi I, Lundström T, Gurin V N and Korusukova M M 2010 *Sci. Technol. Adv. Mater.* in press.
[7] Kuz'ma Yu B, Gurin V N, Korsukova M M, Chaban N F and Chikhrij S I 1988 *Izv. Akad. Nauk SSSR, Neorg. Mater.* **24** 1705
[8] Brandt N B, Gippius A A, Morshchalkov V V, Nyan K K, Gurin V N, Korsukova M M and Kuz'ma Yu B 1988 *Sov. Phys.: Solid State* **30** 797
[9] Korsukova M M, Gurin V N, Kuz'ma Yu B, Chaban N F, Chikhrij S I, Moshchalkov V V, Braudt N B, Gippius A A and Nyan K K 1989 *phys. status solidi a* **114** 265
[10] Korsukova M M, Gurin V N, Yu Y, Tergenius L-E and Lundstrom 1993 *J. Solid State Chem.* **190** 185
[11] Tanaka T, Okada S, Yu Y and Ishizawa Y 1997 *J. Solid State Chem.* **133** 122
[12] Spear K E 1976 *Phase Diagram Vol. IV* (Academic Press, Inc., New York) p 91
[13] Seybolt A U 1960 Trans. Am. Soc. Metals **52** 971
[14] Richards S M and Kasper J S 1969 *Acta Crystallogr. B* **25** 237
[15] Higashi I, Kobayashi K, Tanaka T and Ishizawa Y 1997 *J. Solid State Chem.* **133** 16
[16] Slack G A, Oliver D W, Brower G D and Young J D 1977 *J. Phys. Chem. Solids* **38** 45

[17] Tanaka T *unpublished data*
[18] Tanaka T, Kamiya K, Numazawa, T, Sato A and Takenouchi S 2006 *Z. Kristallogr.* **221** 472
[19] Tanaka T, Okada S and Ishizawa Y 1994 *J. Alloys Compd.* **205** 281
[20] Higashi I 1983 *J. Solid State Chem.* **47** 333
[21] Mori T and Tanaka T 1999 *J. Phys. Soc. JPN.* **68** 2033
[22] Mori T and Tanaka T 1999 *J.Alloys Compd.* **288** 32
[23] Mori T and Tanaka T 2000 *J. Phys. Soc. JPN.* **69** 579
[24] Mironov A, Kazakov S, Jun J and Kapinski J 2002 *Acta Crystallogr.* C**58** 195
[25] Leithe-Jasper A, Tanaka T, Bourgeois L, Mori T and Michiue Y 2004 *J. Solid State Chem.* **177** 431
[26] Zhang F X, Leithe-Jasper A, Xu J, Matsui Y, Tanaka T and Okada S 2001 *J. Solid State Chem.* **159** 174
[27] Zhang F X, Xu F F, Mori T, Liu Q L, Sato A and Tanaka T 2001 *J. Alloys Compd.* **329** 168
[28] Zhang FZ, Xu FF, Leithe-Jasper A, Mori T, Tanaka T, Xu J, Sato A, Bando Y and Matsui Y 2001 *Inorg. Chem.* **40** 6948
[29] Zhang F X, Sato A and Tanaka T 2002 *J. Solid State Chem.* **164** 361
[30] Zhang F X, Xu F F, Mori T, Liu Q L and Tanaka T 2003 *J. Solid State Chem.* **170** 75
[31] Zhang F X and Tanaka T 2003 *Z. Kristallogr. NCS* **218** 26
[32] Tanaka T, Sato A and Zhang F X 2009 *J. Phys.: Conf. Ser.* **176** 012015
[33] Salvador J R, Bilc D, Mahanti S D and Kanatzidis M G 2002 *Angew. Chem. Int. Ed.* **41** 844
[34] Tanaka T and Sato A 2001 *J. Solid State Chem.* **160** 394
[35] Vlasse M, Naslain R, Kasper J S and Ploog K 1979 *J. Less-Common Met.* **67** 1
[36] Higashi I 2000 *J. Solid State Chem.* **154** 1071
[37] Higashi I, Sakurai T and Atoda T 1977 *J. Solid State Chem.* **20** 67
[38] Kasper J S, Vlasse M and Naslain R 1977 *J. Solid State Chem.* **20** 281
[39] Tanaka T, Okada S and Gurin V N 1998 *J. Alloys Compnd.* **267** 211
[40] Shi Y, Leithe-Jasper A and Tanaka T 1999 *J. Solid State Chem.* **148** 250
[41] Leithe-Jasper A, Bourgeois L, Michiue Y, Shi Y and Tanaka T 2000 *J. Solid State Chem.* **154** 130
[42] Tanaka T and Sato A 2002 *J. Solid State Chem.* **165** 148
[43] Leithe-Jasper A, Sato A and Tanaka T 2002 *Z. Kristallogr.-New Crytst. Struct.* **217** 319
[44] Tanaka T, Yamamoto A and Sato A 2002 *J. Solid State Chem.* **168** 192
[45] Tanaka T, Yamamoto A and Sato A 2002 *J. Solid State Chem.* **177** 476
[46] Mori T 2009 *J. Phys.: Conf. Series)* **176** 012036
[47] Wong J, Tanaka T, Rowen M, Schäfers F, Müler BR and Rek ZU 1999 *J. Synchro. Rad.* **6** 1086
[48] Tanaka T, Kamiya K, Numazawa T, Sato A and Takenouchi S 2006 *Z. Kristallogr.* **221** 472
[49] Zarechnaya E Yu, Dubrovinsky L, Dubrovinskaia N, Miyajima N, Filinchuk Y, Chernyshov D and Dmitriev V 2008 *Sci. Technol. Adv. Mater.* **9** 044209
[50] Oganov A R, Chen J, Gatti C, Ma Y, Ma Y, Glass C W, Liu Z, Yu T, Kurakevych O O and Solozhenko V L 2009 *Nature* **457** 863

9. Appendix

Appendix I*a*. Structure data for $YAlB_{14}$ [9].

Atom	Site	x	y	z	Occ.*	$B_{iso.}$(Å^2)
Y	$8i$	0.02511(8)	1/4	0.64217(3)	0.310(1)	Anisotropic
Al	$4c$	1/4	1/4	1/4	0.708(3)	Anisotropic
B1	$8h$	0	0.1660(1)	0.9682(1)	1	0.35(1)
B2	$8h$	0	0.1520(1)	0.3745(1))	1	0.39(1)
B3	$8h$	0	0.0882(1)	0.1704(1)	1	0.35(1)
B4	$16i$	0.1602(1)	0.05917(6)	0.83757(7)	1	0.34(1)
B5	$16j$	0.2482(1)	0.08028(6)	0.45487(8)	1	0.35(1)

*Chemical composition can be calculated as $Y_{0.62}Al_{0.71}B_{14}$.

Appendix I*b*. Anisotropic displacement parameters for $YAlB_{14}$ [9].

Atom	U_{11}(Å^2)	U_{22}(Å^2)	U_{33}(Å^2)	U_{13}(Å^2)
Y	0.087(2)	0.00446(8)	0.00466(8)	-0.00045(9)
Al	0.0112(3)	0.0053(2)	0.0196(3)	0.0108(2)

Appendix II. Structure data for YB_{62} [18].

Atom	Site	x	y	z	Occ.*	$U_{eq.}$(Å^2)
B1	96i	0	0.0374(2)	0.0594(1)	1.0	0.0101(7)
B2	96i	0	0.0759(2)	0.1171(2)	1.0	0.0118(7)
B3	96i	0	0.0387(2)	0.1809(2)	1.0	0.0115(7)
B4	96i	0	0.1486(1)	0.2418(1)	1.0	0.0098(7)
B5	96i	0	0.1855(2)	0.1715(2)	1.0	0.0112(7)
B6	192j	0.0389(1)	0.1401(1)	0.1220(1)	1.0	0.0137(6)
B7	192j	0.0395(1)	0.0816(1)	0.2291(1)	1.0	0.0120(6)
B8	192j	0.0630(1)	0.0775(1)	0.1586(1)	1.0	0.0129(6)
B9	192j	0.0635(1)	0.1455(1)	0.1948(1)	1.0	0.0137(6)
B10	192j	0.1328(3)	0.1744(3)	0.1975(3)	0.758(19)	0.0412(20)
B11	192j	0.2314(4)	0.1607(3)	0.3021(4)	0.531(14)	0.0427(24)
B12	192j	0.1733(4)	0.1273(4)	0.2581(5)	0.293(17)	0.0207(35)
B13	64g	0.2337(8)	0.2337(8)	0.2337(8)	0.076(6)	0.0395(98)
Y1	48f	0.0542(3)	0.25	0.25	0.437(9)	0.0110(9)
Y2	48f	0.0725(11)	0.25	0.25	0.110(12)	0.0414(43)

Appendix III. Structure data for $YB_{41}Si_{1.2}$[a] [4].

Atom	Site	x	y	z	Occ.*	$B_{iso.}$(Å^2)
B1.1	8i	0.4362(2)	0.5491(2)	0.0938(3)	1	0.12(5)
B1.2	8i	0.4660(2)	0.4610(2)	0.1572(3)	1	0.15(5)
B1.3	4g	0.4063(3)	0.4711(3)	0	1	0.19(7)
B1.4	4g	0.4852(3)	0.4078(3)	0	1	0.14(6)
B2.1	8i	0.2326(2)	0.4909(2)	0.0981(3)	1	0.14(5)
B2.2	8i	0.2101(2)	0.3281(2)	0.0956(3)	1	0.13(5)
B2.3	8i	0.1664(2)	0.4147(2)	0.1632(3)	1	0.19(5)
B2.4	8i	0.2749(2)	0.4005(2)	0.1586(3)	1	0.13(4)
B2.5	4g	0.1293(3)	0.3702(3)	0	1	0.11(6)
B2.6	4g	0.1379(3)	0.4694(3)	0	1	0.11(6)
B2.7	4g	0.3106(3)	0.4451(3)	0	1	0.15(7)
B2.8	4g	0.2972(3)	0.3466(3)	0	1	0.20(7)
B3.1	8i	0.3793(2)	0.1879(2)	0.0975(3)	1	0.19(5)
B3.2	8i	0.5354(2)	0.2580(2)	0.0946(3)	1	0.13(5)
B3.3	8i	0.4823(2)	0.1772(2)	0.1640(3)	1	0.11(4)
B3.4	8i	0.4350(2)	0.2693(2)	0.1584(3)	1	0.12(5
) B3.5	4g	0.4501(3)	0.1247(3)	0	1	0.19(6)
B3.6	4g	0.3728(3)	0.2753(3)	0	1	0.28(7)
B3.7	4g	0.4682(3)	0.3146(3)	0	1	0.12(6)
B3.8	4g	0.5424(3)	0.1724(3)	0	1	0.14(6)
B4.1	8i	0.2006(2)	0.1543(2)	0.0880(3)	1	0.16(5)
B4.2	8i	0.1315(2)	0.0978(2)	0.1785(3)	1	0.09(4)
B4.3	8i	0.1156(2)	0.1965(2)	0.1737(3)	1	0.18(5)
B4.4	8i	0.2107(2)	0.2414(2)	0.1753(3)	1	0.15(4)
B4.5	8i	0.2905(2)	0.1676(2)	0.1833(3)	1	0.10(4)
B4.6	8i	0.2377(2)	0.0745(2)	0.1817(3)	1	0.15(4)
B4.7	8i	0.1741(2)	0.0671(2)	0.3370(3)	1	0.23(5)
B4.8	8i	0.0972(2)	0.1445(2)	0.3316(3)	1	0.15(5)
B4.9	84i	0.1508(2)	0.2379(2)	0.3301(3)	1	0.11(4)
B4.10	8i	0.2612(2)	0.2215(2)	0.3352(3)	1	0.15(4)
B4.11	8i	0.2720(2)	0.1169(2)	0.3434(3)	1	0.20(5)
B4.12	8i	0.1884(2)	0.1594(2)	0.4149(3)	1	0.28(5)
B5.1	8i	0.1150(2)	0.4078(2)	0.3354(3)	1	0.19(5)
B5.2	8i	0.1066(2)	0.3127(2)	0.4060(3)	1	0.18(5)
B5.3	8i	0.0255(2)	0.4553(2)	0.4053(3)	1	0.20(5)
B5.4	8i	0.0175(2)	0.3589(2)	0.3358(3)	1	0.18(4)
B5.5	4h	0.4628(3)	0.1121(3)	1/2	1	0.27(7)
B5.6	4h	0.1675(3)	0.3812(3)	1/2	1	0.39(7)
B5.7	4h	0.1202(3)	0.4681(3)	1/2	1	0.31(7)

Appendix III. Continued.

Atom	Site	x	y	z	Occ.*	$B_{iso.}$(Å^2)
B5.8	4h	0.0108(3)	0.3023(3)	1/2	1	0.28(7)
B6.1	8i	0.3311(2)	0.3858(2)	0.3061(3)	1	0.19(4)
B6.2	8i	0.3530(2)	0.4752(2)	0.4064(3)	1	0.35(5)
B6.3	8i	0.4294(2)	0.4214(2)	0.3063(3)	1	0.14(4)
B6.4	8i	0.4150(2)	0.3223(2)	0.3052(3)	1	0.18(4)
B6.5	8i	0.5013(2)	0.3652(2)	0.4046(3)	1	0.20(4)
B6.6	8i	0.3268(2)	0.2925(2)	0.4058(3)	1	0.43(5)
Si6.7[b]	4h	0.2784(3)	0.3866(3)	1/2	0.575(6)	0.22(6)
B6.7[b]	4h	0.2785(13)	0.3961(11)	1/2	0.425(6)	0.22(6)
Si6.8[c]	4h	0.4429(3)	0.2787(3)	1/2	0.478(6)	0.17(7)
B6.8[c]	4h	0.4492(11)	0.2818(12)	1/2	0.522(6)	0.17(7)
Si6.9[d]	4h	0.4655(3)	0.4626(3)	1/2	0.440(6)	0.17(8)
B6.9[d]	4h	0.4589(9)	0.4537(7)	1/2	0.560(60	0.17(8)
B7.1	8i	0.3911(4)	0.3747(4)	0.1181(8)	1	0.30[e]
B7.2	8i	0.3182(17)	0.2183(16)	0.502(31)	0.46(1)	0.30[e]
B7.3	4g	0.4569(3)	0.0212(2)	0	0.23(1)	0.30[e]
B7.4	4g	0.0766(4)	0.1555(6)	0	0.29(1)	0.30[e]
B7.5	4g	0.1438(11)	0.2507(11)	0	0.18(1)	0.30[e]
B7.6	4g	0.2552(10)	0.2629(9)	0	0.43(1)	0.30[e]
B7.7	4h	0.2054(15)	0.0230(14)	1/2	0.08(1)	0.30[e]
Y	8i	0.39628(1)	0.05199(1)	0.22964(3)	1	0.22[f]
Si	4h	0.34402(8)	0.07974(8)	1/2	0.798(6)	0.29[f]

[a] The number n in the atom designation Bn,n refers to the B_{12}-nth icosahedron to which the Bn,n belongs. Si6.n and B6.n belong to the $B_{12}Si_3$ unit. [b,c,d] The Si and B sites are in the same interstice, which is assumed to be fully occupied by both Si and B atoms with occupancies of Occ.(Si) and Occ.(B), respectively, where Occ.(Si)+Occ.(B) = 1. Position of the boron atom was adjusted independently by fixing the thermal parameters at the same value as for the Si atom in the same interstice. [e] The temperature factor is fixed at this value. [f] Equivalent isotropic temperature factor. It was calculated from the relation $B_{eq.} = 4/3(a^2\beta_{11} + b^2\beta_{22} + c^2\beta_{33})$.

Appendix IV. Structure data for homologous compounds.

a. Structure data of $ScB_{15.5}CN$ [25].

Atom	Site	x	y	z	Occ.*	$U_{eq.}$(nm$^2\times10^3$)
Sc	2d	1/3	2/3	0.4426(1)	0.93(1)	16.1(4)
B1	6i	0.4909(4)	0.5091(2)	0.2177(2)	1	3.8(4)
B2	6i	0.5580(1)	0.4420(2)	0.0612(1)	1	3.5(4)
B3	6i	0.7737(2)	0.2263(2)	0.3175(2)	1	4.5(4)
B4	6i	0.8383(4)	0.1617(2)	0.1611(2)	1	4.2(4)
B5	6i	0.8945(2)	0.1055(2)	0.4331(2)	1	4.8(4)
B6	1a	0	0	0	1	5(1)
C	2c	0	0	0.1338(3)	1	4.1(9)
N	2d	1/3	2/3	0.2446(3)	1	6.1(8)

*The sum of those values was fixed at 1.0.

b. Structure data of $YB_{22}C_2N$ [26].

Atom	Site	x	y	z	Occ.*	$B_{iso.}$(Å^3)
Y	6c	0	0	0.349(2)	0.74(4)	0.62(5)
B1	18h	0.223(6)	-0.223(6)	0.442(3)	1.0	2.37(0)
B2	18h	0.557(2)	0.442(8)	0.349(4)	1.0	2.37(0)
B3	18h	0.151(8)	0.303(6)	0.404(3)	1.0	2.37(0)
B4	18h	0.438(0)	0.562(0)	0.379(0)	1.0	2.37(0)
B5	6c	2/3	1/3	0.454(2)	1.01(4)	2.50(4)
B6	18h	0.499(6)	0.500(4)	0.417(5)	1.0	2.37(0)
B7	18h	0.102(1)	-0.102(1)	0.468(5)	1.0	3.37(0)
B8	18h	0.334(9)	0.167(4)	0.494(7)	1.0	2.37(0)
C1	6c	2/3	1/3	0.485(8)	1.16(4)	3.19(0)
C2	6c	2/3	1/3	0.423(2)	0.99(6)	3.19(0)
N	6c	0	0	0.401(3)	0.84(0)	0.95(8)

c. Structure data of $YB_{28.5}C_4$ [27].

Atom	Site	x	y	z	Occ.*	$U_{eq.}(\mathrm{nm}^2\times10^3)$
Y1	6*c*	0	0	0.3200(1)	0.83(9)	7(1)
C2	6*c*	0	0	0.2787(2)	1.12(1)	6(3)
C3	6*c*	2/3	1/3	0.2129(2)	1.06(2)	5(3)
C4	6*c*	2/3	1/3	0.2639(2)	1.05(3)	11(3)
B5	6*c*	2/3	1/3	0.2385(3)	1.12(1)	17(4)
C6	6*c*	1/3	-1/3	0.1922(2)	1.08(5)	11(3)
B7	3*b*	1/3	-1/3	1/6	1.08(0)	13(6)
B8	18*h*	0.1096(8)	-0.1096(8)	0.2265(1)	1.0	2(1)
B9	18*h*	0.2136(17)	0.1068(8)	0.3677(1)	1.0	4(1)
B10	18*h*	0.2177(18)	0.1089(9)	0.1780(1)	1.0	3(1)
B11	18*h*	0.1703(8)	-0.1703(8)	0.1968(1)	1.0	3(1)
B12	18*h*	0.2255(8)	0.4511(17)	0.2498(1)	1.0	3(1)
B13	18*h*	0.4631(17)	0.2316(8)	0.3462(1)	1.0	3(1)
B14	18*h*	0.1632(8)	0.3263(17)	0.2795(1)	1.0	3(1)
B15	18*h*	0.5030(9)	0.4970(9)	0.2690(1)	1.0	4(2)
B16	18*h*	0.3422(17)	0.1711(8)	0.2077(1)	1.0	4(1)
BC17	6*c*	0	0	0.2506(4)	0.51(9)	6(8)

Appendix V*a***.** Structure data for $Y_xB_{12}C_{0.33}Si_{3.0}$ (x=0.68) [32].

Atom	Site	x	y	z	Occ.*	$U_{eq.}$(nm$^2\times10^3$)
Y	9*e*	1/6	1/3	1/3	0.68(1)	6.1(1)
B1	36*i*	0.4916(1)	0.1556(1)	0.1353(1)	1.0	4.5(1)
B2	36*i*	0.3671(1)	0.0400(1)	0.2181(1)	1.0	4.6(1)
B3	18*h*	0.4838(2)	0.2419(1)	0.2307(1)	1.0	7.4(2)
B4	18*h*	0.2900(2)	0.1450(1)	0.2697(1)	1.0	5.1(2)
C3	6*c*	2/3	1/3	0.2666(12)	0.58(5)*	2.9(5)
Si1	6*c*	1/3	2/3	0.2379(0)	1.0	2.7(1)
Si2	18*h*	0.4648(0)	0.5352(0)	0.2730(0)	1.0	4.1(1)
Si3	6*c*	2/3	1/3	0.2917(3)	0.42(2)*	1.1(2)

*The sum of those values was fixed at 1.0.

V*b***.** Interatomic distances between the listed sites of $Y_xB_{12}C_{0.33}Si_{3.0}$ [32].

Atoms	Distance (Å)	Atoms	Distance (Å)
C3-B3	1.703(7)	C3-C3	2.198
Si3-B3	1.887(3)	Si3-C3	0.413
C3-Si3	1.786(24)	Si3-Si3	1.373(10)

Appendix VI. Structure data for $ScB_{19+x}Si_y$ (x=0.7, y=0.18)[a]

Atom	Site	x	y	z	Occ.	$U_{eq.}(nm^2\times10^3)$
B1	8*b*	-0.1228	0.2389	0.1261	1.0	5.06
B(2)	8*b*	-0.0333	0.1355	0.2097	1.0	5.5
B(3)	8*b*	-0.0428	0.3116	0.2294	1.0	5.18
B(4)	8*b*	-0.0398	0.3917	0.1159	1.0	5.36
B(5)	8*b*	-0.0113	0.1129	0.0786	1.0	6.27
B(6)	8*b*	-0.0273	0.272	0.0277	1.0	5.24
B(7)	8*b*	0.1154	0.2258	0.244	1.0	5.93
B(8)	8*b*	0.1027	0.3902	0.192	1.0	5.46
B(9)	8*b*	0.1265	0.1058	0.1548	1.0	5.73
B(10)	8*b*	0.127	0.1951	0.0453	1.0	5.04
B(11)	8*b*	0.1142	0.3624	0.0645	1.0	5.16
B(12)	8*b*	0.2093	0.2618	0.1403	1.0	5.22
B(13)	8*b*	0.3187	0.0588	0.3634	1.0	9.81
B(14)	8*b*	0.3933	0.2069	0.326	1.0	8.95
B(15)	8*b*	0.2135	0.1978	0.3449	1.0	10.19
B(16)	8*b*	0.47	0.1142	0.4131	1.0	6.57
B(17)	8*b*	0.4662	0.2887	0.4239	1.0	6.27
B(18)	8*b*	0.1903	0.0946	0.4509	0.652	9.15
B(19)	8*b*	0.2721	0.1861	0.5453	1.0	6.32
B(20)	8*b*	0.3529	0.042	0.4933	1.0	6.37
B(21)	8*b*	0.4445	0.1865	0.526	1.0	8.9
B(22)	4*a*	0.3354	0.3354	0.5	1.0	8.92
B(23)	4*a*	0.0347	0.0347	0.5	1.0	10.25
B(24)	8*b*	0.3133	0.3367	0.381	0.631	14.73
Sc(1)	8*b*	0.2964	0.4857	0.1316	0.811	4.73
Sc(2)	8*b*	0.2981	0.375	0.2968	0.194	16.22
Sc(3)	8*b*	0.0849	0.0107	0.3215	0.128	5.66
Si	8*b*	0.1758	0.0037	0.4227	0.203	10.09

[a] Obtained by structure analysis.

Appendix VII. Structure data for $ScB_{17}C_{0.25}$.

Atom	Site	x	y	z	Occ.	$U_{eq.}(nm^2\times10^3)$
Sc	12o	0.4251(1)	0.8502(1)	0.7496(2)	1.0	5.8(4)
B1	12p	0.6699(4)	0.7362(4)	0.0	1.0	3.2(9)
B2	12p	0.5300(4)	0.6629(4)	0.0	1.0	6.4(9)
B3	24r	0.5985(3)	0.7380(3)	0.8351(4)	1.0	3.7(7)
B4	12o	0.1419(7)	0.2838(5)	0.9011(6)	1.0	6.6(9)
B5	12o	0.5242(4)	0.2621(2)	0.0986(4)	1.0	4.3(9)
B6	4h	1/3	2/3	0.8288(10)	1.0	5(2)
B7	4h	1/3	2/3	0.6165(10)	1.0	5(2)
B8	24r	0.3077(3)	0.9274(3)	0.6661(4)	1.0	4.4(7)
B9	12g	0.4395(4)	0.0	0.5984(6)	1.0	5.3(8)
B10	12q	0.5375(5)	0.6562(5)	1/2	1.0	6(1)
B11	12n	0.7571(4)	0.0	0.5995(6)	1.0	5.0(9)
B12	12q	0.2266(5)	0.3405(4)	1/2	1.0	6(1)
B13	12o	0.0771(2)	0.1542(5)	0.8347(7)	1.0	4(1)
B14	12n	0.1327(4)	0.0	0.6664(7)	1.0	8(1)
B/C15	6l	0.4694(3)	0.9388(7)	0.0	B/C=0.73/0.27	8(1)
B/C16	6m	0.3944(6)	0.7888(7)	1/2	B/C=0.80/0.20	13(1)
B17	6l	0.0391(12)	0.0782(24)	0.0	0.53	45(8)
B18	6m	0.0379(10)	0.0758(10)	1/2	0.67	44(6)

Appendix VIII. Structure data for $Sc_{0.83-x}B_{10.0-y}C_{0.17+y}Si_{0.083-z}$ ($x = 0.030$, $y = 0.36$ and $z = 0.026$).

Atom	Site	x	y	z	Occ.	$U_{eq.}$(nm$^2\times10^3$)
B1	48h	0.0613(2)	0.0613(2)	0.6638(2)	1.0	6.62
B2	48h	0.1209(2)	0.1209(2)	0.6832(2)	1.0	7.03
B3	48h	0.0864(2)	0.0864(2)	0.5206(2)	1.0	7.83
B4	48h	0.1478(2)	0.1478(2)	0.5438(2)	1.0	8.18
B5	48h	0.1899(2)	0.1899(2)	0.9098(2)	1.0	8.17
B,C6	48h	0.2219(2)	0.2219(2)	0.8378(2)	B/C=0.58/0.42	8.38
B7	48h	0.1068(2)	0.1068(2)	0.8320(2)	1.0	5.93
B8	48h	0.1410(2)	0.1410(2)	0.7596(2)	1.0	6.85
B9	48h	0.3018(2)	0.3018(2)	0.4030(3)	1.0	13.28
B10	48h	0.2191(2)	0.2191(2)	0.9796(3)	1.0	11.33
B11	48h	0.7816(2)	0.7816(2)	0.1217(3)	1.0	13.61
B12	48h	0.3019(2)	0.3019(2)	0.4927(3)	1.0	10.07
B13	96i	0.7693(2)	0.9520(2)	0.1663(2)	1.0	14.96
B14	48h	0.0485(2)	0.0485(2)	0.8212(3)	1.0	7.51
B15	48h	0.0340(2)	0.0340(2)	0.1403(3)	1.0	15.19
B16	96i	0.7875(2)	0.9762(2)	0.0845(2)	1.0	16.48
B17	48h	0.0326(2)	0.0326(2)	0.7384(3)	1.0	14.68
B,C18	16e	0.3494(3)	0.3494(3)	0.3494(3)	B/C=0.51/0.49	9.68
B,C19	16e	0.0623(3)	0.0623(3)	0.0623(3)	B/C=0.85/0.15	12.11
B,C20	16e	0.4447(2)	0.4447(2)	0.4447(2)	B/C=0.73/0.27	8.90
C1	16e	0.1947(3)	0.1947(3)	0.1947(3)	1.0	15.45
Si1	4a	0.2500(0)	0.2500(0)	0.2500(0)	1.0	16.19
Si2	4a	0.5000(0)	0.5000(0)	0.5000(0)	0.38	37.82
Sc1	16e	0.9409(04)	0.9409(04)	0.9409(04)	1.0	8.9[a]
Sc2	16e	0.1270(07)	0.1270(07)	0.1270(07)	0.99	32.99[a]
Sc3	48h	0.0689(04)	0.0689(04)	0.3216(04)	0.95	11.05[a]
	U_{11}	U_{22}	U_{33}	U_{23}	U_{13}	U_{12}
Sc1	8.96	8.96	8.96	-0.91	-0.91	-0.91
Sc2	32.99	32.99	32.99	-9.42	-9.42	-9.42
Sc3	12 .25	12.25	8.65	-0.33	-0.33	-0.12

[a] Anisotropic thermal factors are applied to Sc sites, and U_{eq} (one-third of the trace of the orthogonalized U_{ij} tensor) is listed in these columns.

Appendix IX. Structure data for $Sc_{4.5-x}B_{57-y+z}C_{3.5-z}$ (x =0.27, y = 1.1, z = 0.2).

Atom	Site	x	y	z	Occ.	$U_{eq.}$(nm$^2\times10^3$)
B1	8*i*	0.3347(1)	0.2050(2)	0.6241(2)	1.0	5.8(4)
B2	8*i*	0.1410(2)	-0.1034(2)	0.2728(2)	1.0	6.6(4)
B3	8*i*	0.2612(1)	0.2836(2)	0.6215(2)	1.0	5.8(4)
B4	8*i*	0.4280(1)	0.2589(2)	0.6235(2)	1.0	6.0(4)
B5	8*i*	0.3484(2)	0.2963(2)	0.5582(2)	1.0	5.3(4)
B6	8*i*	0.2823(1)	0.2312(2)	0.7301(2)	1.0	5.4(4)
B7	8*i*	0.3070(1)	0.3795(2)	0.6211(2)	1.0	5.1(4)
B8	8*i*	0.4055(1)	0.3652(2)	0.6226(2)	1.0	5.3(4)
B9	8*i*	0.3898(1)	0.2167(2)	0.7324(2)	1.0	5.8(4)
B10	8*i*	0.3476(2)	0.3034(2)	0.7929(2)	1.0	6.4(4)
B11	8*i*	0.2682(1)	0.3424(2)	0.7236(2)	1.0	5.1(4)
B12	8*i*	0.4371(2)	0.3209(2)	0.7295(2)	1.0	5.9(4)
B13	8*i*	0.4587(2)	-0.0243(2)	0.8542(2)	1.0	7.4(4)
B14	8*i*	0.3552(1)	-0.0209(2)	0.7027(2)	1.0	5.8(4)
B15	8*i*	0.3940(1)	0.0421(2)	0.7953(2)	1.0	5.4(4)
B16	8*i*	0.3019(2)	-0.0052(2)	0.8126(2)	1.0	6.5(4)
B17	8*i*	0.6125(2)	0.1769(2)	0.8143(2)	1.0	6.6(4)
B18	8*i*	0.5250(2)	0.1195(2)	0.7960(2)	1.0	5.9(4)
B19	8*i*	0.0752(2)	0.3872(2)	0.0943(2)	1.0	6.2(4)
B20	8*i*	0.6791(2)	0.1048(2)	0.8810(2)	1.0	6.3(4)
B21	8*i*	0.4539(2)	-0.0273(2)	0.7328(2)	1.0	5.7(4)
B22	8*i*	0.5951(2)	0.1197(2)	0.7028(2)	1.0	6.4(4)
B23	8*i*	0.3716(2)	-0.0065(2)	0.9054(2)	1.0	6.7(4)
B24	8*i*	0.1886(2)	0.3891(2)	0.2408(2)	1.0	6.1(4)
B25	4*h*	0.5570(2)	0.3161(2)	0.5000(0)	1.0	4.8(6)
B26	8*i*	0.5896(2)	0.1702(2)	0.6004(2)	1.0	6.1(4)
B27	4*h*	0.4658(2)	-0.1389(2)	0.5000(0)	1.0	5.9(6)
B28	8*i*	0.6782(1)	0.2169(2)	0.5618(2)	1.0	5.3(4)
B29	4*h*	0.3651(2)	-0.1350(2)	0.5000(0)	1.0	3.4(6)
B30	8*i*	0.5115(1)	0.2348(2)	0.5630(2)	1.0	5.4(4)
C31	4*h*	0.6546(2)	0.3025(2)	0.5000(0)	1.0	7.3(5)
B32	8*i*	0.6020(2)	0.2784(2)	0.6021(2)	1.0	5.7(4)
C33	4*h*	0.1831(2)	0.0261(2)	0.5000(0)	1.0	6.2(5)
C34	4*h*	0.3222(2)	-0.0486(2)	0.5000(0)	1.0	8.9(6)
B35	8*i*	0.2270(2)	0.0603(2)	0.6016(2)	1.0	6.3(4)
B36	8*i*	0.7354(1)	0.5437(2)	0.4379(2)	1.0	6.0(4)
B37	4*h*	0.7189(2)	0.3766(2)	0.5000(0)	1.0	6.4(6)
B38	4*h*	0.3734(2)	0.0459(2)	0.5000(0)	1.0	6.8(6)
B39	8*i*	0.3187(1)	0.0127(2)	0.6004(2)	1.0	5.6(4)

continue Appendix IX.

B40	8*i*	0.3098(2)	0.1178(2)	0.5629(2)	1.0	6.2(4)
B41	8*i*	0.4507(1)	0.4330(2)	0.5607(2)	1.0	5.2(4)
B42	8*i*	0.0390(2)	0.0341(2)	0.6004(2)	1.0	6.1(4)
C43	4*h*	0.5297(2)	0.4086(2)	0.5000(0)	1.0	7.7(6)
B44	4*h*	0.0943(2)	0.0123(2)	0.5000(0)	1.0	5.9(6)
B45	8*i*	0.2050(2)	0.1636(2)	0.7716(2)	1.0	6.0(4)
B46	8*i*	0.0681(2)	0.1263(2)	0.1059(2)	1.0	8.9(5)
B47	8*i*	0.6154(1)	0.3328(2)	0.7019(2)	1.0	5.3(4)
B48	8*i*	0.0749(2)	0.0661(2)	0.7017(2)	1.0	6.7(4)
B49	8*i*	0.1163(2)	0.2096(2)	0.8164(2)	1.0	6.3(4)
B50	8*i*	0.0317(2)	0.1444(2)	0.7735(2)	1.0	6.1(4)
B51	8*i*	0.0415(2)	0.0348(2)	0.1842(2)	1.0	7.5(4)
B52	8*i*	0.1772(1)	0.0777(2)	0.7000(2)	1.0	5.7(4)
B53	8*i*	0.1314(2)	-0.0047(2)	0.2313(2)	1.0	9.2(4)
B54	8*i*	0.1279(2)	0.0314(2)	0.1094(2)	1.0	18.9(6)
B55	8*i*	0.2129(2)	0.0524(2)	0.1870(2)	1.0	7.7(4)
B56	8*i*	0.1744(2)	0.1361(2)	0.1069(2)	1.0	9.2(5)
B57	8*i*	0.7574(2)	0.1419(2)	0.9408(2)	1.0	9.6(5)
B58	4*g*	0.8776(2)	0.2582(3)	0.0000(0)	1.0	9.5(6)
B59	8*i*	0.8460(2)	0.1852(2)	0.9102(2)	1.0	7.4(5)
B60	4*g*	0.2774(2)	0.2621(3)	0.0000(0)	1.0	10.1(7)
B61	4*g*	0.4196(3)	0.3404(3)	0.0000(0)	1.0	17.6(8)
B62	4*g*	0.1589(4)	0.8983(4)	0.0000(0)	0.58	6.0(16)
C/B63	8*i*	0.4300(1)	0.1383(1)	0.7908(2)	C/B=0.80/0.20	6.2(4)
B64	4*g*	0.1305(4)	-0.0080(4)	0.0000(0)	0.78	14.9(15)
C65	4*h*	0.5219(2)	-0.0431(2)	0.5000(0)	1.0	12.6(6)
B66	4*g*	0.9242(3)	0.3500(3)	0.0000(0)	1.0	11.9(7)
B67	4*g*	0.2231(2)	0.1635(2)	0.0000(0)	1.0	8.6(6)
B68	4*g*	0.0246(2)	0.3536(2)	0.0000(0)	1.0	6.8(6)
B69	4*g*	0.5216(2)	0.3482(3)	0.0000(0)	1.0	8.3(6)
B70	4*g*	0.8751(2)	0.4428(3)	0.0000(0)	1.0	10.3(7)
B/Si71	8*i*	0.1440(4)	0.9256(4)	0.0604(4)	B+Si=0.30 (B/Si=0.9/0.1)	6.4(10)
Sc1	8*i*	0.47761(2)	0.24988(3)	0.88052(3)	0.97	6.0(1)[a]
Sc2	2*a*	0.50000(0)	0.50000(0)	0.00000(0)	0.96	14.9(3)[a]
Sc3	8i	0.44587(3)	0.10615(3)	0.63668(3)	0.97	6.2(1)[a]
Sc4	8*i*	0.31793(3)	0.15473(3)	0.87857(3)	0.97	7.1(1)[a]
Sc5	4*g*	0.13723(4)	0.27037(4)	0.00000(0)	0.96	8.8(2)[a]
Sc6	4*g*	0.24837(5)	0.00566(5)	0.00000(0)	0.90	9.3(2)[a]
Sc7	2*c*	0.50000(0)	0.00000(0)	0.00000(0)	0.61	8.3(4)[a]

continue Appendix IX. Anisotropic thermal factors.

Atom	U_{11}	U_{22}	U_{33}	U_{23}	U_{13}	U_{12}
Sc1	5.5(2)	7.6(2)	4.9(2)	-0.8(2)	0.2(1)	0.4(2)
Sc2	14.2(5)	15.2(5)	15.2(5)	0.00	0.00	4.9(4)
Sc3	7.4(2)	5.6(2)	5.5(2)	-0.3(1)	0.3(2)	1.2(1)
Sc4	4.4(2)	11.5(2)	5.4(2)	0.1(2)	0.7(1)	-0.3(2)
Sc5	5.8(3)	11.2(3)	9.5(3)	0.00	0.00	3.0(2)
Sc6	10.3(3)	8.3(3)	9.4(3)	0.00	0.00	-2.6(3)
Sc7	11.3(7)	10.7(7)	2.9(6)	0.00	0.00	-4.6(5)

[a] Anisotropic thermal factors are applied to Sc sites, and U_{eq} (one-third of the trace of the orthogonalized U_{ij} tensor) is listed in these columns.

Appendix X. Structure data for $Sc_{3.67-x}B_{41.4-y-z}C_{0.67+z}Si_{0.33-w}$ (x=0.52, y=1.42, z=1.17 and w=0.02).

Atom	Site	x	y	z	Occ.	$U_{eq.}$(nm$^2\times10^3$)
B1	6*n*	0.8073(5)	0.4037(3)	0.0812(3)	1.0	6.8(10)
B2	6*n*	0.0650(5)	0.5325(2)	0.1400(2)	1.0	6.0(9)
B3	6*n*	0.9269(5)	0.4634(2)	0.0374(2)	1.0	4.4(9)
B4	6*n*	0.9436(5)	0.4718(3)	0.1852(3)	1.0	6.9(10)
B5	12*o*	0.8402(4)	0.3568(3)	0.1453(2)	1.0	7.1(7)
B6	12*o*	0.9843(3)	0.3894(3)	0.1412(2)	1.0	6.0(7)
B7	12*o*	0.0316(3)	0.4545(3)	0.0749(2)	1.0	5.7(7)
B8	12*o*	0.8989(4)	0.3458(4)	0.0781(2)	1.0	7.1(7)
B9	6*n*	0.1969(5)	0.5984(3)	0.1645(3)	1.0	8.0(10)
B10	6*n*	0.2446(5)	0.6223(3)	0.2375(3)	1.0	8.2(11)
B11	6*n*	0.2920(2)	0.5839(5)	0.1205(2)	1.0	5.3(9)
B12	6*n*	0.2647(3)	0.5294(5)	0.1913(2)	1.0	5.7(9)
B13	6*n*	0.2671(59)	0.2671(5)	0.3155(3)	1.0	8.3(10)
B14	6*n*	0.8217(3)	0.1784(3)	0.3748(3)	1.0	12.2(11)
B15	6*n*	0.7742(3)	0.2258(3)	0.2397(2)	1.0	6.1(9)
B16	12*o*	0.7213(4)	0.0679(4)	0.3317(2)	1.0	10.4(8)
B17	12*o*	0.8736(4)	0.3358(4)	0.2828(2)	1.0	8.9(7)
B18	6*n*	0.7304(3)	0.2697(3)	0.2990(3)	1.0	12.0(12)
B19	12*o*	0.9027(4)	0.2288(4)	0.2599(2)	1.0	8.7(7)
B20	12*o*	0.8261(5)	0.3023(5)	0.3556(2)	1.0	17.5(10)
B/C21	6*n*	0.0808(5)	0.0808(5)	0.3880(2)	B/C=0.55/0.45	6.7(9)
B22	6*n*	0.0675(3)	0.0675(3)	0.3478(2)	1.0	6.8(10)
B23	6*n*	0.9185(5)	0.0408(2)	0.2783(2)	1.0	5.8(9)
B24	6*n*	0.9333(3)	0.1334(5)	0.3221(2)	1.0	6.0(10)
B/C25	6*l*	0.3352(5)	0.5516(5)	0.0	B/C=0.55/0.45	6.8(10)
B26	12*o*	0.3193(3)	0.4403(4)	0.0374(2)	1.0	5.8(7)
B27	6*n*	0.1829(2)	0.3658(5)	0.0603(2)	1.0	4.2(9)
B28	6*l*	0.2238(5)	0.3231(5)	0.0	1.0	5.4(9)
B29	6*n*	0.2548(3)	0.5096(5)	0.0612(3)	1.0	6.0(9)
B30	12*o*	0.1777(4)	0.4848(4)	0.3452(2)	1.0	8.9(7)
B31	6*n*	0.2658(3)	0.5316(6)	0.5902(3)	1.0	11.8(11)
B32	6*n*	0.1323(3)	0.2646(5)	0.3660(3)	1.0	7.8(10)
B33	6*n*	0.1854(3)	0.3708(5)	0.3161(3)	1.0	7.7(10)
B34	12*o*	0.0915(4)	0.3082(4)	0.4271(2)	1.0	8.7(7)
B35	12*o*	0.0677(4)	0.3465(4)	0.3582(2)	1.0	9.6(7)
B36	12*o*	0.1183(5)	0.4431(5)	0.4173(2)	1.0	15.6(9)
B37	6*n*	0.2096(3)	0.7905(3)	0.4609(3)	1.0	9.7(11)
B/C38	6*m*	0.0027(5)	0.1179(5)	0.5	B/C=0.65/0.35	6.8(9)
B39	6*m*	0.7666(5)	0.1089(5)	0.5	1.0	6.9(10)

continue Appendix X.

B40	12*o*	0.9869(4)	0.2146(4)	0.4628(2)	1.0	7.4(7)
B/C41	6*n*	0.9211(2)	0.1578(5)	0.4421(2)	B/C=0.45/0.55	7.1(9)
B42	6*n*	0.8514(3)	0.1486(3)	0.4387(3)	1.0	6.7(9)
B43	6*l*	0.2387(5)	0.2133(5)	0.0	1.0	6.4(10)
B44	12*o*	0.8843(3)	0.2383(3)	0.0392(2)	1.0	6.0(7)
B45	3*j*	0.1431(7)	0.0716(3)	0.0	1.0	3.3(13)
B46	6*n*	0.2359(5)	0.1180(2)	0.0579(2)	1.0	4.6(9)
B47	6*n*	0.1969(3)	0.3938(6)	0.1835(3)	1.0	12.4(12)
B48	6*n*	0.1543(3)	0.3086(5)	0.1262(2)	1.0	6.0(10)
B49	12*o*	0.0178(4)	0.2465(4)	0.2240(2)	1.0	9.9(8)
B50	6*n*	0.0872(2)	0.1745(5)	0.2267(2)	1.0	6.6(9)
B51	12*o*	0.0563(4)	0.3250(4)	0.1626(2)	1.0	8.7(7)
B52	6*n*	0.1530(3)	0.3060(6)	0.2517(3)	1.0	13.3(12)
B53	12*o*	0.1623(3)	0.1884(3)	0.1601(2)	1.0	5.9(7)
B54	6*m*	0.4507(8)	0.3567(8)	0.5	1.0	27.0(18)
B55	12*o*	0.4300(9)	0.9827(9)	0.4547(4)	0.87	43.8(29)
B56	6*n*	0.5907(5)	0.4093(5)	0.3925(5)	0.66	17.7(32)
B57	6*n*	0.8050(13)	0.4025(7)	0.4762(6)	0.51	16.9(40)
B58	12*o*	0.5007(9)	0.3781(9)	0.4206(5)	0.44	12.2(28)
B59	6*n*	0.8881(16)	0.4440(8)	0.4595(8)	0.55	30.9(53)
C60	2*i*	0.6667	0.3333	0.7126(5)	1.0	15.9(21)
B61	1*a*	0.0	0.0	0.0	1.0	10.5(27)
B62	6*n*	0.1877(5)	0.5939(3)	0.3066(3)	1.0	9.4(11)
C63	6*n*	0.7421(2)	0.2579(2)	0.1798(2)	1.0	8.6(9)
B/C64	6*n*	0.9344(5)	0.4672(2)	0.2578(2)	B/C=0.57/0.43	6.2(10)
B65	6*n*	0.9172(3)	0.0828(3)	0.1237(3)	1.0	6.1(9)
B66	1*f*	0.6667	0.3333	0.5	1.0	43.4(68)
B/C67	2*h*	0.3333	0.6667	0.5774(5)	B/C=0.71/0.29	10.5(22)
B68	2*i*	0.6667	0.3333	0.0639(4)	1.0	5.0(16)
B69	2*h*	0.3333	0.6667	0.3006(8)	0.49	0.0(44)
Si1	2*i*	0.6667	0.3333	0.3919(2)	0.87	30.7(16)
Si2	2*i*	0.6667	0.3333	0.2078(1)	1.0	5.0(5)
Sc1	2*g*	0.0	0.0	0.17777(8)	0.98	5.5(4)^a
Sc2	3*j*	0.74237(6)	0.74237(6)	0.0	0.95	7.0(4)^a
Sc3	6*n*	0.07873(4)	0.07873(4)	0.06563(4)	0.96	4.5(2)^a
Sc4	12*o*	0.07726(8)	0.43056(8)	0.24776(3)	0.87	9.4(2)^a
Sc5	6*n*	0.82732(5)	0.82732(5)	0.14302(6)	0.96	19.5(4)^a
Sc6	6*n*	0.50007(6)	0.50007(6)	0.35580(6)	0.91	14.4(3)^a
Sc7	3*k*	0.40577(10)	0.40577(10)	0.5	0.88	31.1(9)^a
Sc8	6*n*	0.74848(9)	0.25152(9)	0.45210(9)	0.49	6.3(5)^a

continue Appendix X. Anisotropic thermal factors.

Atom	U_{11}	U_{22}	U_{33}	U_{23}	U_{13}	U_{12}
Sc1	4.7(5)	4.7(5)	7.1(8)	0.0	0.0	2.4(3)
Sc2	8.5(6)	8.5(6)	7.3(6)	0.0	0.0	6.8(6)
Sc3	4.6(3)	4.6(3)	4.1(4)	0.2(2)	0.2(2)	2.1(4)
Sc4	7.0(4)	8.5(4)	11.6(3)	4.2(3)	1.4(3)	3.1(2)
Sc5	26.9(6)	26.9(6)	18.2(6)	2.8(2)	2.8(2)	23.6(7)
Sc6	13.6(5)	13.6(5)	16.4(6)	0.1(2)	0.1(2)	7.1(5)
Sc7	15.0(9)	15.0(9)	66.7(21)	0.0	0.0	10.3(9)
Sc8	4.9(7)	4.9(7)	7.9(9)	0.8(3)	0.8(3)	1.7(7)

[a] Anisotropic thermal factors are applied to Sc sites, and U_{eq} (one-third of the trace of the orthogonalized U_{ij} tensor) is listed in these columns.